Design, Synthesis, and Pharmacological Evaluation of N-Acylhydrazones and Novel Conformationally Constrained Compounds as Selective and Potent Orally Active Phosphodiesterase-4 Inhibitors

Arthur E. Kümmerle,[†,‡,||] Martine Schmitt,[§] Suzana V. S. Cardozo,[▽,¶] Claire Lugnier,[△] Pascal Villa,[#] Alexandra B. Lopes,[†,‡] Nelilma C. Romeiro,[▼] Hélène Justiniano,[△] Marco A. Martins,[▽] Carlos A. M. Fraga,[†,¶] Jean-Jacques Bourguignon,[§,⊥] and Eliezer J. Barreiro*[,†,⊥]

[†]Laboratório de Avaliação e Síntese de Substâncias Bioativas (LASSBio), Faculdade de Farmácia, Universidade Federal do Rio de Janeiro, Rio de Janeiro 68023, RJ 21944-971, Brazil

[‡]Programa de Pós-Graduação em Química, Instituto de Química, Universidade Federal do Rio de Janeiro, 21941-902, Rio de Janeiro, RJ, Brazil

[§]Laboratoire d'Innovation Thérapeutique, UMR7200, CNRS, Université de Strasbourg, Faculté de Pharmacie, 74 Route du Rhin, 67400 Illkirch-Graffenstaden, France

[▽]Laboratório de Inflamação, Departamento de Fisiologia e Farmacodinâmica, Instituto Oswaldo Cruz-Fiocruz, Rio de Janeiro, RJ, Brazil

[¶]Programa de Pós-Graduação em Farmacologia e Química Medicinal, Instituto de Ciências Biomédicas, Universidade Federal do Rio de Janeiro, 21941-902 Rio de Janeiro, RJ, Brazil

[△]Biophotonique et Pharmacologie, UMR7213, CNRS, Université de Strasbourg, Faculté de Pharmacie, 74 Route du Rhin, 67400 Illkirch-Graffenstaden, France

[#]Plate-forme de Chimie Biologie Integrative de Strasbourg (PCBIS), UMR3286, CNRS, Université de Strasbourg, Ecole Supérieur de Biotechnologie et Faculté de Pharmacie, Boulevard Sebastien Brant, 67412 Illkirch-Graffenstaden, France

[▼]Universidade Federal do Rio de Janeiro (UFRJ)-Macaé-Rua Aluísio da Silva Gomes, 50 Granja dos Cavaleiros, 27930-560 Rio de Janeiro, RJ, Brazil

Ⓢ *Supporting Information*

ABSTRACT: Among a small series of tested N-acylhydrazones (NAHs), the compound **8a** was selected as a selective submicromolar phosphodiesterase-4 (PDE4) inhibitor associated with anti-TNF-α properties measured both *in vitro* and *in vivo*. The recognition pattern of compound **8a** was elucidated through molecular modeling studies based on the knowledge of the 3D-structure of zardaverine, a PDE4 inhibitor resembling the structure of **8a**, cocrystallized with the PDE4.

Based on further conformational analysis dealing with N-methyl-NAHs, a quinazoline derivative (**19**) was designed as a conformationally constrained NAH analogue and showed similar *in vitro* pharmacological profile, compared with **8a**. In addition **19** was found active when tested orally in LPS-evoked airway hyperreactivity and fully confirmed the working hypothesis supporting this work.
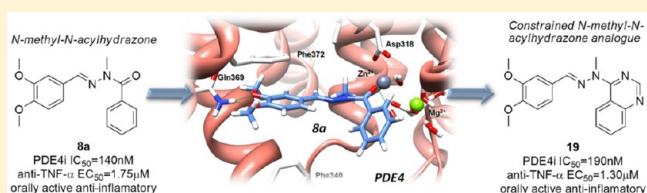
INTRODUCTION

Phosphodiesterases (PDEs) play a critical role in maintaining the cellular levels of cyclic adenosine monophosphate (cAMP) and cyclic guanosine monophosphate (cGMP).[1−4] Cellular biological responses such as secretion, contraction, metabolism, and growth are mediated by levels of these ubiquitous second messengers.[5]

PDEs are responsible for the hydrolysis of phosphodiester bonds in cAMP and cGMP,[6] and in humans, PDEs can be subdivided into 11 different groups or isozymes, PDE1 to PDE11.[7,8]

Among these, the multigene phosphodiesterase-4 (PDE4)[9,10] family has attracted considerable attention over the past decade because PDE4 is found in many cell types and tissues, including leukocytes, airway and vascular smooth muscle, vascular endothelium, and brain.[9] The involvement of PDE4 in

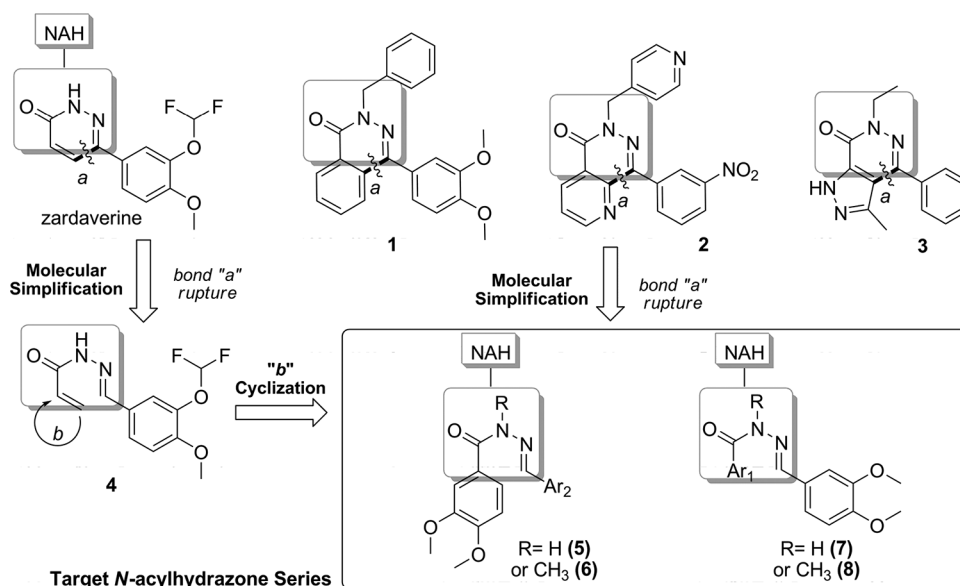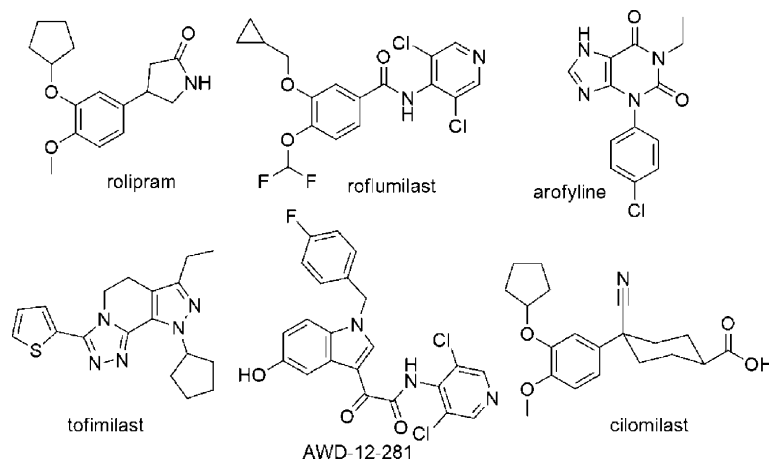**Chart 1. Chemical Structures of Different PDE4 Inhibitors**

Figure 1. Structural design of the target NAH series **5–8**.

pathological processes associated with these tissues suggests a great potential for pharmacological intervention in a variety of inflammatory, vascular, angiogenic, and neurological disorders through modulation of cAMP levels.[7,9] Potential therapeutic use of PDE4 inhibitors deal with various therapies including asthma, allergic rhinitis, atopic dermatitis, chronic obstructive pulmonary disease (COPD), rheumatoid arthritis, psoriasis, Crohn's disease, cancer, Alzheimer's disease, mild cognitive impairment, Parkinson's disease, schizophrenia, and depression.[11–19]

Over the past decade, the number of studies dealing with the modulation of cAMP or cGMP levels through the action of PDE have increased dramatically; the relevance of modulating PDE activity has been demonstrated by the high number of selective PDE inhibitory drug candidates that have been synthesized and tested in clinical trials for different inflammatory disorders such as asthma and COPD (Chart 1).[20]

While some of these drugs appeared to be promising (e.g., roflumilast[21–24] and tofimilast[25]), many were discontinued from development because of the potential overlap of efficacy and undesired side effects such as nausea and emesis.[20] These adverse side effects were thought to be due to the inhibition of

PDE4 in nontarget tissues, notably in the CNS and the gut.[26] It was further hypothesized that these side effects were either caused by activating emetic centers within the CNS or by binding at a high-affinity allosteric binding site on PDE4 (called the rolipram binding site)[27] affecting gastric acid-secreting cells in the gut. Another proposal emphasized inhibition of a specific PDE4 gene, most probably PDE4D, as the source of emetic effects of PDE4 inhibitors.[17,26,28,29]

Despite possible side effects, the lack of alternative treatments for inflammatory disorders such as COPD continues to stimulate research efforts leading to discovery of new safer PDE4 inhibitors, which have been further encouraged by the recent approval of roflumilast for use in treating this disease.[30]

In this paper, we describe the design, synthesis, pharmacological profile, and molecular modeling of a novel combinatory class of *N*-acylhydrazone (NAH) derivatives and a number of NAH structurally related heterocyclic compounds that may act as PDE4 inhibitors. NAH derivatives have been extensively described by our group[31] as potent anti-inflammatory, antinociceptive, antiplatelet, and vasoactive compounds and characterized as a privileged structure.[32]

Scheme 1[a]
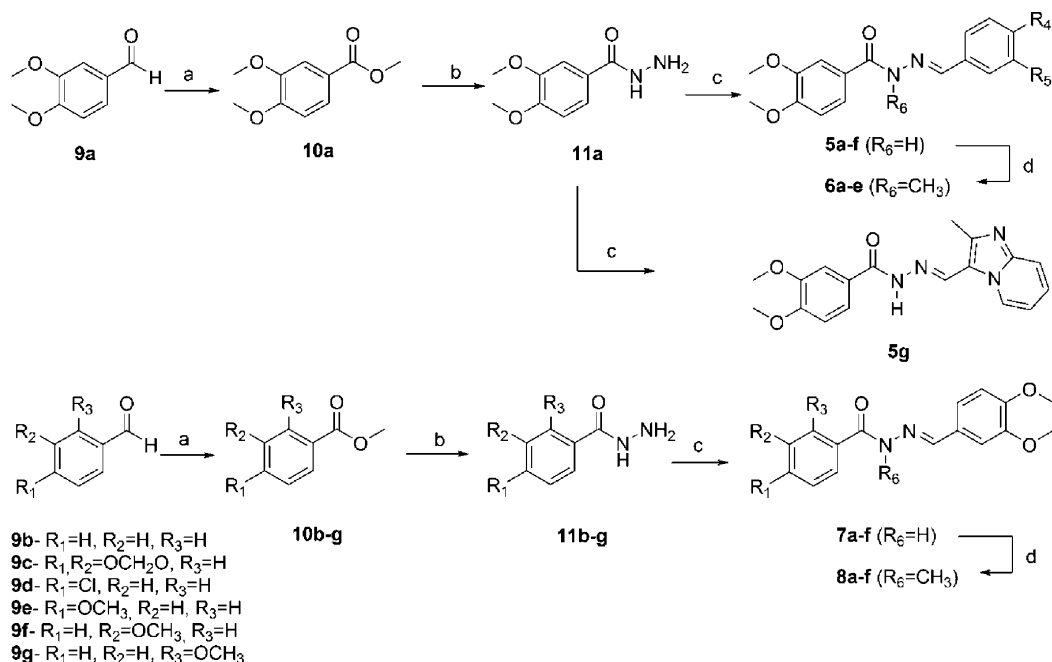
[a]Reagents and conditions: (a) I_2, KOH, MeOH, 0 °C, 2 h, 83−92%; (b) $NH_2NH_2 \cdot H_2O$, EtOH, 70 °C, 3 h, 82−92%; (c) Ar−CHO, EtOH, HCl_{cat}, rt, 1.5 h, 71−97%; (d) CH_3I, K_2CO_3, acetone, 50 °C, 24 h, 75−98%.

Previously, our group described the strategy of molecular simplification of PDE inhibitors[33] using a simple bond rupture between positions 5 and 6 of the central pyridazinone ring, which allowed us to identify the structural similarities between these cardioactive compounds and NAH derivatives.[34] These studies led to the discovery of LASSBio-294, a potent positive cardio-inotropic agent that increases Ca^{2+} accumulation in the sarcoplasmic reticulum (SR)[35] and acts as a vasodilating agent in aortic rings. These effects are mediated through the guanylate cyclase/cyclic guanylate monophosphate pathway.[36]

Because the *N*-acylhydrazone chemotype has a bioisosteric relationship with the pyridazinone ring, which is shared by the PDE4 inhibitors zardaverine and compounds **1**−**3**,[37,38] the same strategy of molecular simplification, represented by a simple bond rupture in **a** and a cyclization step in **b**, was used for the design of this novel series (Figure 1). The pharmacophoric elements needed for PDE4 activity, that is, the catechol ring, was successively linked to both to the acyl (Ar₁, compounds **5** and **6**) and the imine (Ar₂, compounds **7** and **8**) groups. Finally, we selected a set of aryl groups Ar₁ and Ar₂, including phenyl, 3,4-dimethoxyphenyl, 4-chlorophenyl, 2-, 3-, or 4-methoxyphenyl, 4-hydroxyphenyl, and 2-methylimidazo[1,2-*a*]pyridinyl. The selection was based on the following physical criteria: σ-Hammett constant (−0.4 to +0.3), molar refractivity (25−39 cm^3/mol), lipophilic profile, and ability to be an acceptor or donor of hydrogen. The 3,4-methylenedioxyphenyl group was also selected to test potential bioisosterism with the catechol moiety. We also explored the influence of *N*-methyl substitution (R = H or Me) on activity. This strategy was later successfully utilized by our group to synthesize a potent vasodilatory NAH,[39,40] which confirmed that the *N*-methyl group markedly changed the conformation of *N*-acylhydrazone group.[39]

RESULTS AND DISCUSSION

Chemistry. The synthesis of the target NAH series **5**−**8** was carried out according to the procedures depicted in Schemes 1−3. The compounds **5a**−**g** and **7a**−**f** were synthesized from the corresponding acylhydrazines **11a**−**g** that were obtained from the oxidative processing of aldehydes **9a**−**g**, as described by Yamada,[41] who used iodide in potassium hydroxide methanolic solution followed by a hydrazinolysis reaction using hydrazine hydrate in ethanol and resulted in global yields ranging from 70% to 93%.[42] Thus, the compounds **5a**−**g** and **7a**−**f** were prepared via acid-catalyzed condensation of **11a**−**g** with the corresponding aromatic aldehydes with high yields of 71% to 97% (Scheme 1).

The phenolic NAH derivative **7g** was obtained by trying a number of successive classical functional group interconversions on aldehyde **9h**, which could not be converted to the corresponding ester by the previously employed Yamada's oxidation.[41] Thus, the treatment of **9h** with sodium cyanide and manganese oxide in methanol at room temperature[43] provided the ester **10h** with a 71% yield. The hydrazinolysis of the methyl ester **10h** afforded the corresponding hydrazide **11h** in 80% yield. Condensation of **11h** with 3,4-dimethoxybenzaldehyde furnished the new NAH derivative **7g** in 61% yield (Scheme 2).

Finally, the 2-methylimidazo[1,2-*a*]pyridinyl derivative NAH **7h** was synthesized through the synthesis sequence shown in Scheme 3, resulting in a high overall yield. The imidazo[1,2-*a*]pyridine derivative **13** was obtained with a 79% yield using regioselective cyclocondensation of 2-aminopyridine **12** with ethyl 2-chloro-acetoacetate in absolute ethanol at reflux (Scheme 3).[44,45] The successive hydrazinolysis and acid-catalyzed condensation of **12** with 3,4-dimethoxybenzaldehyde gave the desired 2-methylimidazo[1,2-*a*]pyridinyl NAH **7h** with a 72% yield, as previously described. It is worth mentioning that some compounds of the **5** and **7** series described herein can be
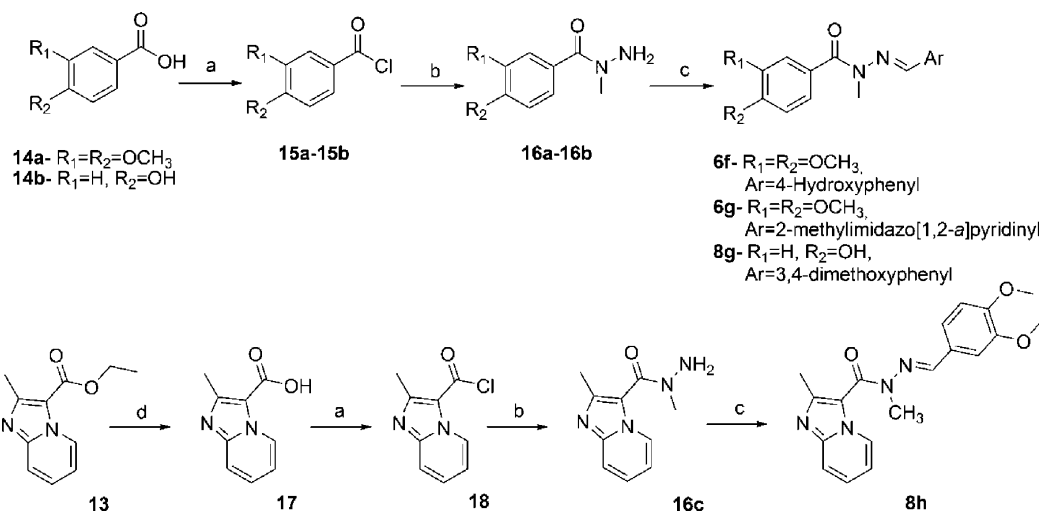
Scheme 2[a]
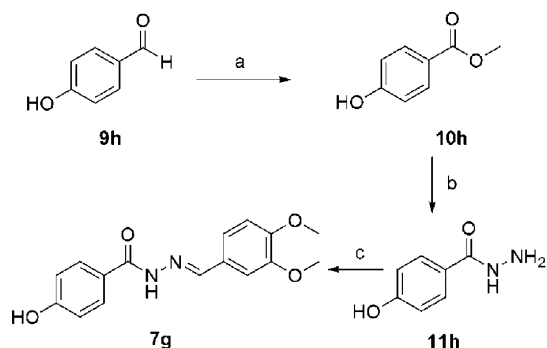
[a]Reagents and conditions: (a) MnO₂, NaCN, MeOH, 24 h, rt, 71%; (b) NH₂NH₂·H₂O, EtOH, 70 °C, 3 h, 80%; (c) 3,4-dimethoxybenzaldehyde, EtOH, HCl_cat, rt, 1.5 h, 61%.

Scheme 3[a]
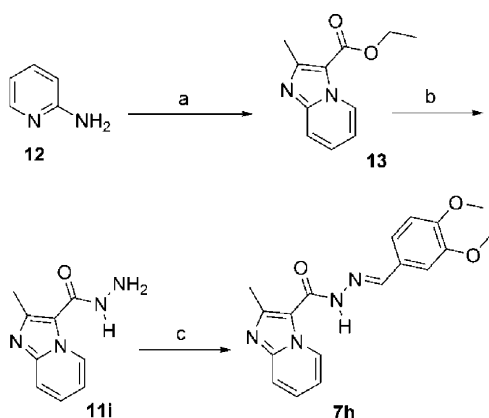
[a]Reagents and conditions: (a) ethyl 2-chloro-acetoacetate, EtOH, reflux, 20 h, 79%; (b) NH₂NH₂·H₂O, EtOH, 70 °C, 3 h, 84%; (c) 3,4-dimethoxybenzaldehyde, EtOH, HCl_cat, rt, 1.5 h, 72%.

found in other studies with different routes of synthesis and biological activities distinct from those intended here.[46−48]

Careful analysis of the ¹H NMR spectra of the NAH derivatives **5a−g** and **7a−h** allowed us to detect the formation of a single isomer based on the presence of a single imino hydrogen signal, which was attributed to the (*E*)-isomer. Several previous reports by our group described this configuration of bioactive *N*-acylhydrazone derivatives, as determined through ¹H NMR and crystallographic analyses.[39,49−51]

Next, the *N*-methyl-NAH series **6a−e** and **8a−f** were synthesized in yields ranging from 75% to 98% using selective *N*-methylation of the corresponding *N*-acylhydrazones **5a−e** and **7a−f** following treatment with potassium carbonate in acetone and the addition of methyl iodide (Scheme 1).[39,52]

¹H NMR analysis confirmed the selective *N*-alkylation based on the absence of signal relative to the N**H** amide of *N*-acylhydrazones and by the presence of a *N*-methyl singlet signal ranging from δ 3.52 to δ 3.58.

The *N*-methyl phenolic (**6f**, **6g**, **8g**) and 2-methylimidazo[1,2-*a*]pyridinyl (**8h**) NAHs could not be synthesized by the previously described *N*-methylation method due to the presence of other groups presenting other nucleophilic groups. These *N*-methyl-NAH were obtained from the corresponding *N*-methylhydrazides **16a−c** and were synthesized in good yields (82−90%) by slowly adding a diluted solution of acid chloride **15a−c** (0.15 M in dichloromethane) in a solution 10 equiv of *N*-methylhydrazine in dichloromethane at 0 °C (Scheme 4).[53] The ¹H NMR analysis facilitated the confirmation of the regioselective formation of *N*-methyl-benzohydrazides **16a−c** based on the lack of characteristic signal normally associated with the amide N**H** proton, around δ 9.0 to 10.0. This is typical of unmethylated hydrazides, as observed for **11a−i**, in addition to the presence of signal associated with the hydrazide amino group, which accounts for two hydrogens ranging from δ 3.91 to δ 4.85.

Careful analysis of the ¹H NMR spectra of the new *N*-acylhydrazone derivatives described herein allowed us to detect a unique regioisomer, based on the presence of a single *N*-methyl signal and the presence of only one imino hydrogen signal, which was attributed to the (*E*)-isomer, as described in

Scheme 4[a]

14a- R₁=R₂=OCH₃
14b- R₁=H, R₂=OH

15a-15b

16a-16b

6f- R₁=R₂=OCH₃, Ar=4-Hydroxyphenyl
6g- R₁=R₂=OCH₃, Ar=2-methylimidazo[1,2-*a*]pyridinyl
8g- R₁=H, R₂=OH, Ar=3,4-dimethoxyphenyl

13   **17**   **18**   **16c**   **8h**

[a]Reagents and conditions: (a) SOCl₂, DMF_cat, 70 °C, 4 h; (b) CH₃NHNH₂, CH₂Cl₂, 0 °C, 3 h, 79−91% (global yield a, b); (c) Ar−CHO, EtOH, HCl_cat, rt, 1.5 h, 82−90%; (d) KOH, MeOH/H₂O 70 °C, 5 h, 98%.

several previous reports by our group identifying the configuration of bioactive N-acylhydrazone derivatives.[39,42]

The heterocyclic compounds **19–21** were obtained as depicted in Schemes 5–7. The quinazoline derivative **19** was
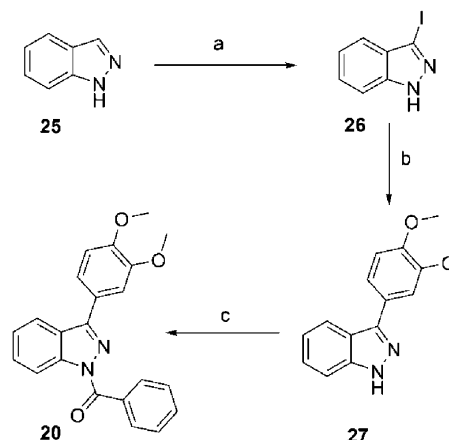
Scheme 5[a]
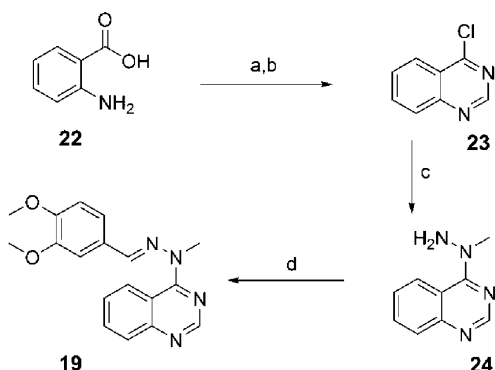
[a]Reaction conditions: (a) formamidine acetate, EtOH, microwave, 130 °C, 40 min, 89%; (b) POCl₃, 110 °C, 2 h, 86%; (c) CH₃NHNH₂, CH₂Cl₂, 0 °C, 3 h, 96%; (d) 3,4-dimethoxybenzaldehyde, EtOH, HCl_cat, rt, 1.5 h, 81%.

synthesized starting from the cyclization of anthranilic acid **22** with formamidine acetate under microwaves, followed by a chlorination reaction with phosphorus oxychloride yielding the 4-chloroquinazoline **23**. Hydrazinolysis of **23** with a diluted solution of N-methylhydrazine at 0 °C, as previously described,[53] afforded the compound **24**, which was subsequently condensed with 3,4-dimethoxybenzaldehyde in ethanol and gave the desired quinazoline **19** with a 81% yield. The presence of only one imino hydrogen signal at δ 7.92 in its ¹H NMR spectrum supported the formation of the single (E)-isomer.

Halogenation of the indazole **25** with iodine in presence of potassium hydroxide led to the formation of 3-iodoindazole **26**, which was subsequently reacted with 3,4-dimethoxyphenylboronic acid under microwaves, in a Suzuki cross-coupling reaction using tetrakis palladium as a catalyst (Scheme 6). A regioselective acylation of **27** was performed with benzoyl chloride in pyridine solution to yield the desired indazolyl derivative **20**.

The benzo[1,2-d]-diazepin-1-one derivative **21** was obtained as described in Scheme 7. The 2-trimethylsilanylethynyl-benzoate **28** was prepared according to a previously published procedure,[54] followed by a Sonogashira cross-coupling reaction with 4-bromo-1,2-dimethoxybenzene using bis-(triphenylphosphine)palladium(II) chloride as a catalyst under microwave irradiation. This procedure yielded the acetylene **29**,[54,55] which was then cyclized with trifluoroacetic acid in a 6-endo-dig mechanism leading to the isocoumarone **30**.[55] Finally **30** was reacted with hydrazine hydrate or methylhydrazine to produce the final 2,3-benzodiazepinones **21** or **22**, respectively.

PDE4 Inhibition. The different N-acylhydrazones and their structurally related compounds were tested for their capacity to inhibit PDE4. The activity was measured using PDE4 isolated from the media layer of bovine aorta, according to a previously reported method with modifications, which was shown to be similar to the PDE4 isolated from human aorta.[56,57] PDE activity was measured using a previously described[58] two-step

Scheme 6[a]

[a]Reagents and conditions: (a) I₂, KOH, DMF, 1 h, 88%; (b) 3,4-dimethoxyphenylboronic acid, Pd(Ph₃)₄, Na₂CO₃, DME/H₂O, microwave, 155 °C, 30 min, 64%; (c) benzoyl chloride, pyridine, 8 h, 74%.
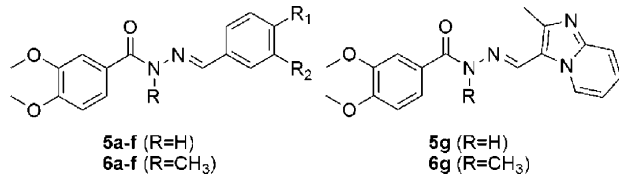
Scheme 7[a]
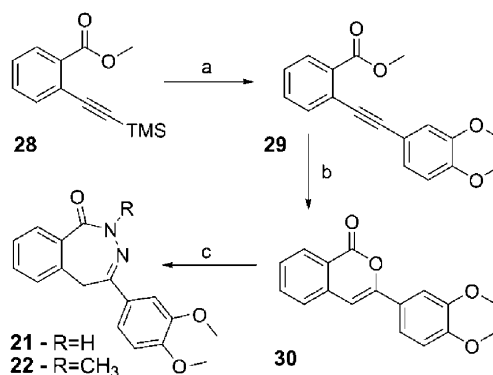
[a]Reagents and conditions: (a) 4-bromo-1,2-dimethoxybenzene, PdCl₂(PPh₃)₂, PPh₃, CuI, piperidine, K₂CO₃, THF/MeOH (7:1), 80 °C, 15 h, 85%; (b) TFA, rt, 0.5 h, 91%; (c) NH₂NH₂·H₂O or CH₃NHNH₂, n-BuOH, 90 °C, 5 h, 87% and 82%.

assay at 1 μM cAMP. The results are summarized in Tables 1 and 2.

The nonmethylated NAH compounds **5a–g** and **7a–h** showed almost no inhibition of PDE4 catalytic activity (IC₅₀ > 10 μM) (Tables 1 and 2). Conversely, N-methylation of these compounds yielding the N-methyl-NAH series **6** and **8** has led to quite different results. Among these N-methyl-NAH derivatives, the PDE4 inhibitory activity was strongly modulated by substituent effects at both Ar₁ and Ar₂. SAR analysis also allowed us to reach a number of other comments:

(i) Within the compound **6** series (Ar₂ = 3,4-dimethoxyphenyl), the inhibitory activity emerged when Ar₁ was another 3,4-dimethoxyphenyl group (**6b**, IC₅₀ = 0.3 μM), whereas all the other derivatives (**6a**, **6c–6e**) were inactive. Only the para-methoxy derivative **6e** showed some inhibitory activity with an IC₅₀ close to 10 μM.

(ii) When the compound **8** is considered, the second series of N-methyl-NAH was the most promising and showed compounds with IC₅₀'s ranging from 50 to 290 nM. Interestingly the derivative **8a** bearing a nonsubstituted Ar₁ ring was relatively potent. These results clearly highlighted the critical role played by the 3,4-

Table 1. PDE4 Inhibition of NAH Derivatives from Series 5 and 6

5a-f (R=H)
6a-f (R=CH₃)

5g (R=H)
6g (R=CH₃)

compd	R	R₁	R₂	% inhib[a]	IC₅₀[b] (nM)
				PDE4	
rolipram					800
5a	H	H	H	5.8	c
5b	H	OCH₃	OCH₃	10.7	c
5c	H	OCH₂O		10.5	c
5d	H	Cl	H	6.4	c
5e	H	OCH₃	H	6.6	c
5f	H	OH	H	1.5	c
5g	H			7.7	c
6a	CH₃	H	H	22.8	c
6b	CH₃	OCH₃	OCH₃	95.8	300
6c	CH₃	OCH₂O		19.8	c
6d	CH₃	Cl	H	40.4	c
6e	CH₃	OCH₃	H	45.8	c
6f	CH₃	OH	H	27.0	c
6g	CH₃			23.7	c

[a]Percent inhibition of PDE4 activity after incubation with the target compound at a drug concentration of 10 μM. [b]The IC₅₀ was calculated by nonlinear regression and represents the mean value of three measurements; the experimental error is approximately 15%. [c]IC₅₀ was not determined when % inhibition was <50% at 10 μM.

Table 2. PDE4 Inhibition of NAH Derivatives from Series 7 and 8

7a-g (R=H)
8a-g (R=CH₃)

7h (R=H)
8h (R=CH₃)

compd	R	R₁	R₂	R₃	% inhib[a]	IC₅₀[b] (nM)
					PDE4	
rolipram						800
7a	H	H	H	H	13.1	c
7b	H	OCH₂O		H	16.0	c
7c	H	Cl	H	H	7.5	c
7d	H	OCH₃	H	H	9.7	c
7g	H	OH	H	H	13.6	c
7h	H			H	41.5	c
8a	CH₃	H	H	H	97.1	140
8b	CH₃	OCH₂O		H	96.3	110
8c	CH₃	Cl	H	H	97.0	150
8d	CH₃	OCH₃	H	H	98.3	105
8e	CH₃	H	OCH₃	H	98.1	290
8f	CH₃	H	H	OCH₃	97.8	210
8g	CH₃	OH	H	H	98.4	50
8h	CH₃			H	45.9	c

[a]Percent inhibition of PDE4 activity after incubation with the target compound at a drug concentration of 10 μM. [b]The IC₅₀ was calculated by nonlinear regression and represents the mean value of three measurements; the experimental error is approximately 15%. [c]IC₅₀ was not determined when % inhibition was <50% at 10 μM.

Table 3. PDE4 Recombinant Isoform Inhibition (IC₅₀, nM) for Selected Compounds 8d and 8g

compd	PDE4A	PDE4B	PDE4C	PDE4D
rolipram, 23	162	231	3690	622
8d	159	53	505	74
8g	64	47	206	31

dimethoxyphenyl fragment when it was located close to the imine function (Ar₂) and the importance of the N-methylation of the NAH series. As previously demonstrated, the N-methylation of amides in NAH leads to conformational changes that may markedly modify pharmacological behaviors,[39,59] as shown by our results.
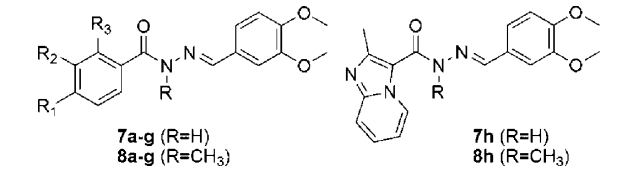
(iii) Within the same series, the presence of a *para*-phenolic OH group on Ar₁ slighty increased the potency (one-third of magnitude order), yielding a compound **8g** with an IC₅₀ of 50 nM, when compared with **8a**.

The two most active compounds in inhibiting PDE4 in bovine aorta extract were **8d** and **8g**. Based on the existence of four isoforms of PDE4, that is, PDE4A, PDE4B, PDE4C, and PDE4D, these two compounds were evaluated for their selectivity against the human PDE4 subtypes. From the IC₅₀ values shown in Table 3, neither **8d** nor **8g** presented any significant selectivity profile, in particular, PDE4B/PDE4D profile.

According to Houslay et al.,[9] PDE4 isoforms are involved in various physiological processes. Although PDE4B is likely related to the modulation of TNF-α biosynthesis, the PDE4D isoform and, to some extent, the PDE4A isoform are primarily implicated in the positive regulation of pulmonary hyperreactivity induced by allergens.[9] According to a recent review by Kodimuthali,[20] the PDE4C isoform is not normally found in pro-inflammatory cells. Thus, the increased activity of these compounds against subtypes B and D, as observed with **8d** and **8g**, may represent an important characteristic profile for anti-inflammatory effects.

On the other hand, PDE4 inhibitors cause undesirable effects such as nausea and vomiting, which strongly limit their

therapeutic potential.[60] In ferrets, established as an appropriate animal species to assess emetic response in preclinical settings, PDE4 inhibitors induce vomiting reflex via a noradrenergic pathway in the central nervous system.[61] Reversal of the hypnotic effect of the α2-adrenoceptor agonist xylazine has proven to be a useful alternative model to evaluate the emetic potential of PDE4 inhibitors in nonvomiting species such as rodents.[26,62] In the current study, we noted that compounds **8d** and **8g** did not reduce the duration of anesthesia triggered by the xylazine/ketamine association in A/J mice, different from what was observed following rolipram treatment as shown in Figure 2. These results confirm previous findings pointing out the pro-emetic profile of the prototype compound rolipram in this system[61] and strongly suggest that the class of N-methyl-N-acylhydrazones, represented by **8d** and **8g**, shows much promise for an anti-inflammatory therapeutic application: their inhibitory effects on PDE4B and PDE4D associated with a lack of effect on xylazine-induced anesthesia, which is an indicative of the low potential to trigger emesis.

Because PDE exists as 11 different families or isozymes involved in various physiological processes,[7,8] the selective inhibition of PDE4 is important to consider when trying to minimize possible side effects. Thus we carried out selectivity
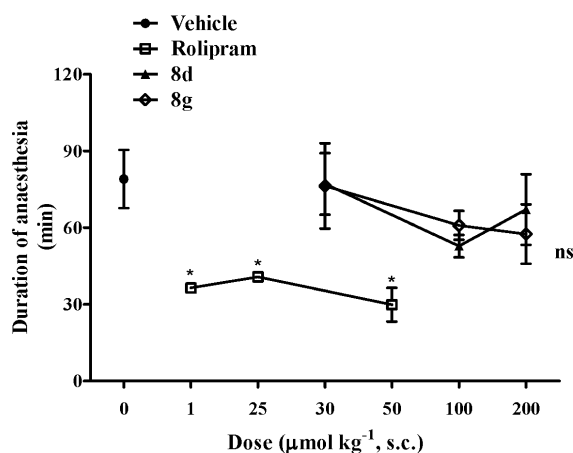
Figure 2. Effect of subcutaneous administration of **8d** or **8g** (30−200 μmol/kg), rolipram (1−50 μmol/kg), or vehicle (0.2% Tween 80) on the duration of anesthesia induced by the combination of xylazine (10 mg/kg) and ketamine (70 mg/kg) in A/J mice. Values are represented as mean ± SEM from at least six mice. *$P < 0.05$ compared with the vehicle group.

profiling of compounds **6b** and **8a−g** toward the PDE1−PDE6 isoforms (Table 4). Data revealed that all compounds displayed a minimal selectivity index ranging from 16- to 182-fold, calculated from the highest IC_{50} found with the PDE1, PDE2, PDE3, PDE5, and PDE6 isoforms in comparison to the IC_{50} obtained for the PDE4 isoform.

A literature analysis dealing with structural diversity of known PDE inhibitors showed that several classes possessed the 3,4-dimethoxyphenyl fragment in their structure, which was also associated with moderate PDE4/PDE3 selectivity. Controlling the selectivity toward PDE3 was generally found to be the most challenging but may be significantly increased by small substituent effects as shown in our series of NAH, when **8a** and **8b** or **8g** are compared. Interestingly, compound **8d** (Ar_1 = 4-MeO-Ph) was active toward both the PDE4 and PDE5 with IC_{50}'s close to 100 nM.

TNF-α Inhibition. Among the growing list of pro-inflammatory mediators known to be involved in pathologies such as arthritis,[63] AIDS, and asthma, tumor necrosis factor-α (TNF-α) may be of particular importance in initiating chronic inflammation through its promotion of cytokine secretion from a variety of cells.[64,65] TNF-α is mainly produced by cells of the monocyte/macrophage lineage. PDE4 inhibitors have been shown to inhibit lipopolysaccharide (LPS)-induced TNF-α

production in monocytes.[66] In addition, the archetypal selective PDE4 inhibitor rolipram and other PDE4 inhibitors display inhibitory effects on LPS-induced TNF-α release in human whole blood.[67]

We selected compounds **6b** and **8a−g** to further evaluate their *in vitro* anti-inflammatory activities by examining the suppression of TNF-α release by lipopolysaccharide (LPS)-activated peripheral blood mononuclear cells from healthy donors (Table 5). These compounds elicited strong inhibition of TNF-α release with EC_{50}'s ranging from 0.52 (**8g**) to 1.75 μM (**8a**).

Table 5. Suppression of TNF-α Release by LPS for Selected Compounds

compd	% inhibition of TNF-α at 10 μM	$EC_{50}{}^a$ (μM)
rolipram		0.13
6b	92	1.18 ± 0.10
8a	91	1.75 ± 0.82
8b	90	0.54 ± 0.04
8c	88	1.03 ± 0.1
8d	84	1.45 ± 0.21
8e	81	1.27 ± 0.14
8f	80	1.59 ± 0.14
8g	83	0.52 ± 0.04

^{a}The EC_{50} was calculated by linear regression (correlation coefficient r = 0.95) and represents the mean value of three measurements; the experimental error is approximately 15%

The compound **8g** has been identified as more potent in inhibiting both PDE4 activity and the TNF-α release. No correlation was found between PDE4 inhibition and TNF-α inhibition for compounds **6b** and **8a−f**. Although **8d** and **8g** displayed similar potency in inhibiting PDE4D, with IC_{50}'s of 53 and 47 nM, respectively, **8g** was almost 3-fold more potent than **8d** in inhibiting TNF-α production. These findings may be attributed to the differences in the physicochemical properties between these compounds, such as cell permeability or water solubility, or they may suggest that accumulation of cAMP is an important mechanism in decreasing TNF-α secretion but is certainly not the only one. In particular, the kinome offers numerous protein kinases involved in multiple transduction signaling pathways in cells.

It is noteworthy that many protein kinase inhibitors acting as ATP competitors may present strong pharmacophoric similarities with PDE4 inhibitors, in particular an H-bond

Table 4. Selectivity Profile of NAH Derivatives 6b and 8a−g against PDE Subtypes

	% inhibition^a at 10 μM or $IC_{50}{}^b$					
compd	PDE1	PDE2	PDE3	PDE5	PDE6	fold selectivity (PDEX/PDE4)
6b	38.7%	40.8%	18.8 μM	30.9%	17.6 μM	59
8a	6%	23.5%	19.6 μM	22.3%	31.2%	140
8b	0%	4.0%	19.4%	5.1%	0.6%	>90
8c	17.7%	26.6%	6.7 μM	27.5%	34.0%	45
8d	25.1%	35.5%	6.7 μM	0.15 μM	35.2%	1.5
8e	18.5%	40.4%	4.5 μM	29.1%	39.5%	16
8f	11.0%	16.8 μM	6.2 μM	13.9%	11.0%	26
8g	28.3%	39.3%	11.8 μM	27.9%	9.1 μM	182

^{a}Percent inhibition of the PDE1, PDE2, PDE3, PDE,5 and PDE6 isoform activities after incubation with the target compound at a drug concentration of 10 μM. ^{b}The IC_{50} was calculated by nonlinear regression and represents the mean value of three measurements; the experimental error is approximately 15%.

Table 6. Effect of a Single Oral Administration of Either 45 μmol/kg Rolipram (10 mg/kg) or Selected Compounds (100 μmol/kg, 30−35 mg/kg, Oral) on the LPS-Induced Generation of TNF-α and IL-6 in the Lung Tissue 18 h Postchallenge (*in Vivo*)

stimulus	treatment	TNF-α^a (pg/mg)	inhibition (%)	IL-6^a (pg/mg)	inhibition (%)
saline	vehicle	5.3 ± 1.4		7.5 ± 1.7	
LPS	vehicle	17.0 ± 1.8^b		37.0 ± 3.0^b	
	+ rolipram	8.9 ± 1.3^c	69	20.9 ± 2.8^c	54
	+ 6b	8.3 ± 0.3^c	74	17.7 ± 2.6^c	65
	+ 8a	11.6 ± 1.4^c	46	21.2 ± 2.3^c	53
	+ 8b	7.6 ± 1.7^c	80	10.0 ± 1.8^c	92
	+ 8c	10.7 ± 1.6^c	54	19.7 ± 3.7^c	59
	+ 8d	11.0 ± 1.1^c	51	23.8 ± 2.7^c	45
	+ 8e	8.2 ± 2.8^c	75	25.8 ± 4.1^c	38
	+ 8f	5.3 ± 0.8^c	100	7.9 ± 1.5^c	99
	+ 8g	12.9 ± 2.4	35	35.2 ± 2.7	6

^{a}Values represent the mean ± SEM from at least four animals. LPS (25 μg/25 μL) was administered intranasally. ^{b}P < 0.05 compared with saline-stimulated and saline-treated mice. ^{c}P < 0.05 compared with LPS-stimulated and saline-treated mice.

Table 7. Effect of a Single Oral Administration of Either 45 μmol/kg Rolipram (10 mg/kg) or Selected NAH Derivatives (100 μmol/kg, 30−35 mg/kg, Oral) on LPS-Induced Accumulation of Total Leukocytes and Neutrophils in the Bronchoalveolar Space 18 h Postchallenge

stimulus	treatment	total leukocytes^a ($\times 10^3$/BAL)	inhibition (%)	neutrophils^a ($\times 10^3$/BAL)	inhibition (%)
saline	vehicle	65.8 ± 3.9		3.1 ± 1.0	
LPS	vehicle	480.5 ± 46.2^b		416.0 ± 40.7^b	
	+ rolipram	191.3 ± 39.7^c	70	128.1 ± 30.0^c	70
	+ 6b	262.5 ± 10.0^c	53	209.2 ± 6.7^c	50
	+ 8a	177.1 ± 14.5^c	73	136.2 ± 14.5^c	68
	+ 8b	222.9 ± 32.5^c	62	138.3 ± 23.4^c	67
	+ 8c	192.9 ± 26.6^c	69	193.1 ± 31.5^c	54
	+ 8d	145.0 ± 9.7^c	81	136.6 ± 7.9^c	68
	+ 8e	179.7 ± 17.6^c	73	99.4 ± 11.2^c	77
	+ 8f	264.6 ± 23.5^c	52	197.0 ± 11.3^c	53
	+ 8g	211.9 ± 28.4^c	65	167.2 ± 26.4^c	60

^{a}Values represent the mean ± SEM from at least five animals. ^{b}P < 0.05 compared with saline-stimulated and saline-treated mice. LPS (25 μg/25 μL) was administered intranasally. ^{c}P < 0.05 compared with LPS-stimulated and saline-treated mice.

acceptor−donor system (NAH) surrounded by aromatic groups (Ar$_1$ and Ar$_2$). This comment supports the hypothesis that some of our compounds may act as multitarget drugs.

***In Vivo* Pulmonary Hyperreactivity Assays.** Compounds presenting the most favorable pharmacological *in vitro* profiles were then investigated *in vivo*. A murine model of acute lung inflammation and airway hyperresponsiveness was used to conduct a primary screening of the oral activity of the selected compounds in an efficacy comparison to rolipram.[68] A/J mice were challenged intranasally with LPS (25 μg/25 μL) and were given 100 μmol/kg (30−35 mg/kg) of compounds 6b and 8a−g by gavage 1 h before provocation. The reference compound rolipram (10 mg/kg), cilomilast (3 mg/kg), and the vehicle (0.2% Tween-80) were also tested under the same conditions. As expected from previous findings,[69] rolipram inhibited LPS-induced TNF-α and IL-6 production in lung tissue by 69% and 54%, respectively, whereas 6b inhibited these cytokines by 74% and 65%, respectively (Table 6). Moreover, cilomilast almost abolished TNF-α and IL-6 generation (84% and 100% inhibition, respectively; Table S1, see Supporting Information). Concerning the tested compounds, higher inhibitory potency was exhibited by compounds 8f and 8b for both TNF-α (100% and 80%) and IL-6 (99% and 80%), respectively (Table 6). Since it is not feasible to increase the rolipram dosing in A/J mice without inducing significant toxic effects, our findings suggest that the selected *N*-methyl-NAH derivatives (6b, 8f,

and 8b) are more effective than rolipram and as effective as cilomilast in the *in vivo* setting. We also found that compounds 8a and 8c−f provided protective effects comparable to those of rolipram, whereas 8g failed to prevent TNF-α and IL-6 production in the lung tissue. This finding differs from that obtained *in vitro* by using the PBMC system, in which 8g was the most potent compound (Table 5). The lack of *in vivo* activity of 8g, despite the marked PDE4 inhibitory capacity and anti-TNF-α potency (IC$_{50}$ = 50 nM and EC$_{50}$ = 520 nM, respectively; Tables 2 and 5), is likely due to physicochemical properties, including cell permeability and water solubility of this compound. Further investigation in this area is ongoing.

Intranasal administration of LPS induces strong lung inflammation, with macrophage activation and recruitment of neutrophils to the interstitium, alveoli, and airways of mice.[70,71] As shown in Table 7, LPS stimulation led to a significant accumulation of leukocytes in the bronchoalveolar space, characterized predominantly by neutrophil infiltration (87%). Mononuclear cells and eosinophils were also present but in lower proportions (8% and 5%, respectively; data not shown). Significant neutrophil infiltration of the lungs of A/J mice following LPS stimulation has been documented in prior studies.[72] This result is also consistent with findings in other mouse models[73,74] and in other species, including rats,[74] rabbits,[71] dogs,[75] pigs,[76] sheep,[77] and primates.[78] Lung neutrophilia induced by LPS is associated with the upregulation

Table 8. Effect of a Single Oral Administration of Either 45 μmol/kg Rolipram (10 mg/kg) or Selected NAH Derivatives (100 μmol/kg, 30−35 mg/kg, Oral) on LPS-Evoked Airway Hyperreactivity (Changes in Lung Resistance and Lung Elastance) 18h Postchallenge Following Provocation with Increasing Aerosolized Concentrations of Methacholine (0, 3, 9, and 27 mg/mL)

stimulus	treatment	resistance[a] (AUC$_{0-27}$)	inhibition (%)	elastance[a] (AUC$_{0-27}$)	inhibition (%)
saline	vehicle	202.0 ± 21.0		9676 ± 1150	
LPS	vehicle	496.8 ± 28.0[b]		25677 ± 1978[b]	
	+ rolipram	218.1 ± 28.9[c]	95	10315 ± 2123[c]	96
	+ 6b	224.5 ± 46.7[c]	92	13101 ± 2479[c]	79
	+ 8a	325.2 ± 35.8[c]	58	17410 ± 1199[c]	51
	+ 8b	332.8 ± 28.3[c]	56	15376 ± 1870[c]	64
	+ 8c	400.5 ± 23.4[c]	33	14189 ± 1606[c]	72
	+ 8d	318.4 ± 47.2[c]	61	15753 ± 2862[c]	62
	+ 8e	290.2 ± 30.8[c]	70	14704 ± 3738[c]	69
	+ 8f	316.4 ± 32.6[c]	61	16249 ± 1941[c]	59
	+ 8g	392.1 ± 38.6[c]	36	15863 ± 3170[c]	61

[a]Values are shown as area under the curve formed following treatment with aerosolizaed methacholine, containing concentrations ranging from 0 to 27 mg/mL (AUC$_{0-27}$), capturing both lung resistance and elastance. Values represent the mean ± SEM from at least four animals. LPS (25 μg/25 μL) was administered intranasally. [b]$P < 0.05$ compared with saline-stimulated and saline-treated mice. [c]$P < 0.05$ compared with LPS-stimulated and saline-treated mice.

of vascular cell adhesion molecules and increased discharge of neutrophilic granules. This system has been used to study intervention strategies for several pathologies including sepsis, acute lung injury, acute respiratory distress syndrome, asthma, and COPD.[78−80] In the present study, we showed that 10 mg/kg rolipram caused a inhibition of 70% in LPS-induced neutrophilia (Table 7) and also reduced mononuclear and eosinophil numbers (data not shown). In another set of experiments, 3 mg/kg cilomilast led to a 43% blockade of the LPS-induced neutrophil infiltration into the airway space (Table S1, see Supporting Information). The maximum inhibition of LPS-induced neutrophilia by rolipram was similar to that observed with other highly potent PDE4 inhibitors such as GSK256066 and roflumilast in LPS models of lung inflammation.[81,82] Similar to rolipram, 6b and 8a−g significantly inhibited (50−77%) LPS-induced lung neutrophilia. Some of these compounds, 8a, 8d, and 8e inhibited the total leukocyte and neutrophil infiltration to a greater degree than the reference compounds rolipram (Table 7) and cilomilast (Table S1, see Supporting Information).

Bronchial hyperreactivity, defined as increased airway responsiveness to nonspecific bronchoconstrictor agents, is a pivotal characteristic of asthma and a well-established marker of the severity of this disease. Administration of LPS into the airways of mice leads to early bronchopulmonary hyper-reactivity, which is independent of both TNF-α synthesis and neutrophil infiltration into murine lungs.[83] To examine the effect of 6b and 8a−g on LPS-induced airway hyperreactivity, we measured airway resistance and elastance in anaesthetized and mechanically ventilated mice using the invasive whole-body plethysmography technique. Provocation with aerosolized methacholine of mice subjected to LPS-intranasal instillation clearly upregulated lung baseline levels of airway resistance and elastance, and these changes were clearly sensitive to cilomilast (100−93% inhibition) and rolipram (95−96% inhibition), as shown in Table S1 (Supporting Information) and Table 8, respectively. Compound 6b was shown to be almost as effective as the references in preventing LPS-induced airway hyper-reactivity; all selected compounds, including 8g, showed significant inhibition of this parameter.

Molecular Modeling. Molecular modeling studies were carried out to examine the molecular basis of PDE4 inhibitory

activity by N-methyl-NAH compounds and to investigate the pharmacophoric role of the 3,4-dimethoxyphenyl group connected to the imine function. This study was performed with compound 8a, because it does not have substituents on the phenyl ring linked to the amide function and it shows no significant difference in its IC$_{50}$ compared with the other compounds (higher than 1 or 2 orders of magnitude). Only E-isomers were evaluated in this study because of the experimental evidence of the configuration of the substituents on the imine group.

Molecular Docking. The binding interactions were determined by docking the inhibitors in the active site. The FlexX molecular docking program[84] interfaced with Sybyl 7.3 (tripos.com) on a Linux Red Hat v.5 workstation was employed to find possible interactions of N-methyl-NAH inhibitors and the PDE4 active site. FlexX is an automated docking program based on incremental construction that accounts for ligand flexibility by changing the conformations of the ligand in the active site while making the protein rigid.

The crystal structure of zardaverine bound to human PDE4D was used (PDB ID code 1XOR; resolution 1.54 Å).[85] The choise of this PDE4D was based on the direct correlation of its cocrystallized compound (zardaverine) and our NAH series, and the highly conserved amino acid sequence of both PDE4 genes (B and D). Although the compounds have been tested on bovine smooth muscle PDE4, the high homology among PDE4s in mammals including PDE4A, B, C, D genes led us to expect similar results for human PDE4, which was confirmed in the current study. Amber F99 charges[86] and hydrogen atoms were assigned in the Biopolymer module, available in Sybyl 7.3. The active site was defined at approximately 8.0 Å from the cocrystallized ligand, zardaverine, and care was taken to cover the important residues Gln369 and Phe372 and also the Zn^{2+} and Mg^{2+} metal ions. The default FlexX scoring function was used to rank order the docked conformational groups, and the best-docked result for each group was then used to analyze the binding interactions.

Molecular Conformation Considerations. The 30 best ranked poses observed for 8a and PDE4 presented score values ranging from −24.44 to −19.90 kJ/mol and showed some similarities in the conformational diversity. Thus, they have been split into three major groups of conformers (Figure 3),
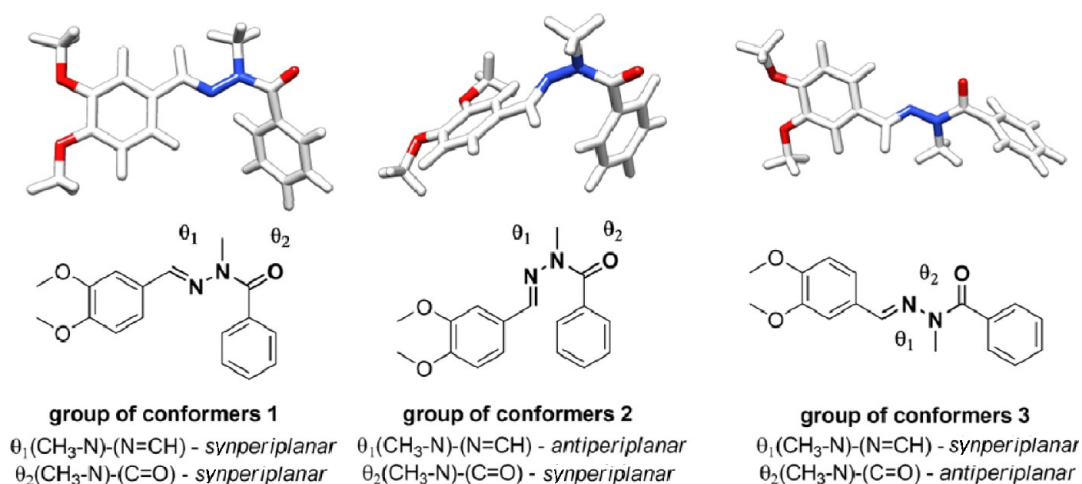
Figure 3. Groups of conformers obtained through visual analysis from the molecular docking study.

and their best energies for each group and for zardaverine are depicted in Table 9. There were only small free energy

Table 9. FlexX Scores for Groups 1−3 on PDE4D

compound	FlexX score[a]	IC_{50}[b] (nM)
zardaverine	−29.55	800
8a (group 1)	−21.87	140
8a (group 2)	−24.44	140
8a (group 3)	−22.12	140

[a]FlexX score in kJ/mol. [b]The IC_{50} was calculated by nonlinear regression and represents the mean value of three independent measurements. The experimental error is approximately 15%.

differences observed among the three groups of conformations, and there was no direct correlation between potency and FlexX score obtained for zardaverine and 8a, indicating that no group could be excluded.

The first group presented the methyl bridged to the amide function in a *synperiplanar* position related to the carbonyl oxygen and the methylidene of the imine. In the second group, the methyl was in a *synperiplanar* position with respect to oxygen and in an *antiperiplanar* position to the imine methylidene. In the third group, the methyl was *antiperiplanar* to the methyl and *synperiplanar* compared with methylidene (Figure 3).

Analysis of the Binding Cavity Access. Binding cavity access analysis was conducted to observe the binding modes and to correlate them with enzyme inhibition.

Group 1 binds to the enzyme and blocks the entrance of the catalytic site, including the region where catalytic water molecules and metal ions are located (Figure 4). Judging from visual inspection of the inhibitor−PDE4 complex, the insertion of substituents in the aromatic ring linked to the carbonyl group would not jeopardize the interaction of the *N*-methyl-NAH function with amino acid residues in the active site, thereby supporting the inhibition profile of these compounds.

Group 2 shows a binding position around the catalytic site but without a complete blockage of the catalytic water molecules and metal ions (Figure 4). Nevertheless, it could be hypothesized that this position would be effective in blocking cAMP entrance, because this conformation is bulky
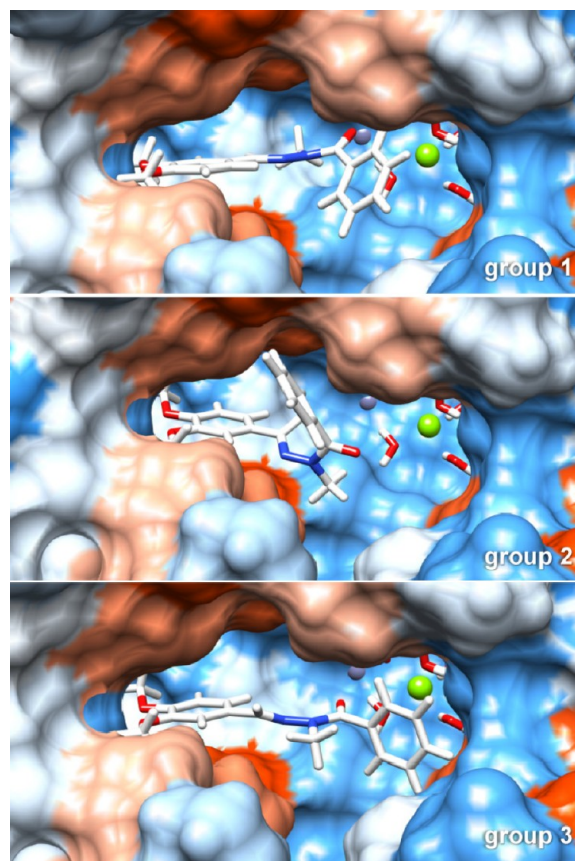

Figure 4. Binding cavity of PDE4D with the docked groups 1, 2, and 3. Docking studies were performed by using the program FlexX.[84]

and the interior of the binding site is closely associated with the *N*-methyl-NAH chain.

The analysis of group 3 shows an excellent hypothetical interaction with the binding site of PDE4. However, the introduction because of the aromatic ring linked to the carbonyl would not be tolerated because they would lie in a sterically hindered region, unavailable for new substituents (Figure 4). Additionally, the *antiperiplanar* orientation of the methyl group related to the oxygen carbonyl is not considered to be stable for *N*-methyl-NAH compounds, as observed in X-ray crystallography of methylated compounds.[39,87] Finally, the *antiperiplanar*
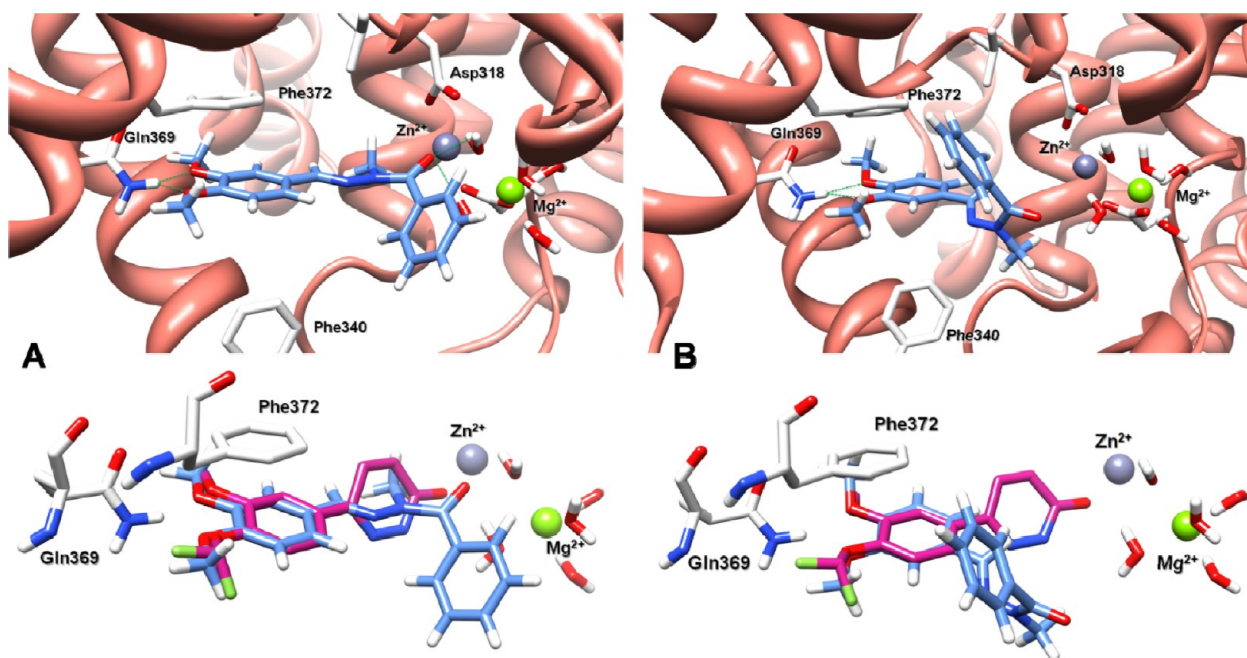
Figure 5. (A) Binding interactions of group 1 of **8a** (blue) with PDE4D (top) and its superposition with zardaverine (violet) inside the catalytic site (bottom). (B) Binding interactions of group 2 of **8a** (blue) with PDE4D (top) and its superposition with zardaverine (violet) inside the catalytic site (bottom). Docking studies were performed by using the program FlexX.[84]

orientation is more favorable in compounds that present secondary amide bonds, such as observed in NAH **5a–g** and **7a–f**. However, these compounds have not shown any significant PDE4 inhibition. Therefore we can conclude that group 3 compounds could not be real.

Molecular Basis of the Interactions of Conformers from Groups 1 and 2 with PDE4. Molecular docking allowed us to compare the binding interactions of the conformer groups 1 and 2 and of zardaverine and their surroundings by the amino acid residues in the catalytic site. A 3D analysis shows that group 1 conformers have a significant superimposition with zardaverine (Figure 5A), in which the 3,4-dimethoxyphenyl and acylhydrazone groups of group 1 and zardaverine occupy the same space in the catalytic site and are involved in the same type of interactions. Both ether oxygen atoms of the 3,4-dimethoxyphenyl moiety of zardaverine and the group 1 conformers are involved in bifurcated hydrogen bonds to the side chain of Gln369 and perform π-stacking with Phe372. Additionally, the carbonyl group of **8a** interacts with Zn^{2+} via a water molecule, while zardaverine chelates the metal ion directly (Figure 5A).

Group 2 conformers interact in the binding site of PDE4D in a similar manner as the conformers from group 1, characterized by hydrogen bonding of the 3,4-dimethoxyphenyl group and Gln369 and π-stacking with Phe372 (Figure 5B). However, different from group 1, group 2 does not fill the binding pocket in the same region as the acylhydrazone chain of zardaverine. Instead, the *N*-methyl-NAH chain is oriented to the exterior, positioning the aromatic ring linked to the carbonyl group at the entrance of the catalytic site. Thus, the carbonyl does not interact with the metal ions, which is mandatory for inhibitory activity, and the aromatic ring is located in a sterically open region, which might be occupied by substituted aromatic rings without interfering in the activity profile.

The two binding modes considered so far may be correlated to the inhibitory activities toward PDE4 *in vitro* (Table 9). As observed by docking studies, all *para*-substituents in Ar₁ fall into a region without steric hindrance, where they cannot perform new interactions with the catalytic site (see Ar₁ *para*-position on Figures 4 and 5). Perhaps the differences in activities found between these compounds is due to the effects of solvation and desolvation or electronic effects generated on the carbonyl group, which is responsible for interaction with the water in the region of the metals. Apparently, donor groups such as −OH and −OMe led to an increase in activity with respect to -H, while -Cl slightly reduced the activity. Substituents *ortho*- and *meta*-OMe in Ar₁, in turn, could find regions with slightly more steric hindrance, as is visible in Figures 4 and 5, and also could result in reorientation of the aromatic ring, which slightly reduces its activity but does not perceptibly changed the theoretical results. In fact, the binding mode evaluation of other compounds in the series with similar inhibition profiles has shown similar docking poses (data in Supporting Information).

Design of Conformationally Restricted NAHs and Their Pharmacological Evaluation. Based on the molecular docking studies of **8a**, two possible interactions with the catalytic site were proposed (Figure 5). There are two possible bioactive conformations, as previously described by our group.[88] We have designed a set of four different NAH structurally related compounds to validate the theoretical results and propose new scaffolds for PDE4i activity (Figures 6 and 7).

As illustrated in Figure 6, the semifolded conformation from group 1 provided the quinazoline **19** by bridging the carbonyl oxygen onto the *ortho* position of the benzamide (mode a) and the indazole **20** resulted from the incorporation of the hydrazine into a pyrazole ring system (mode b). Conversely, because of the folded conformation from group 2, the 2,3-benzodiazepinones **21** and **22** were designed by bridging the imine carbon onto the *ortho* position of benzamide through a methylene group (mode c) (Figure 7).
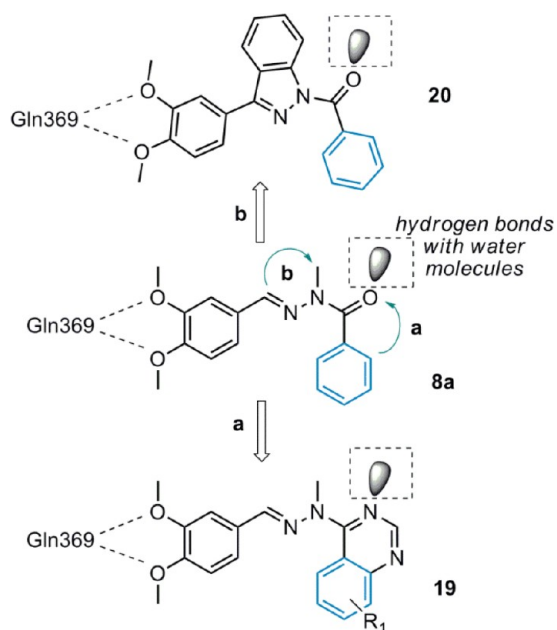
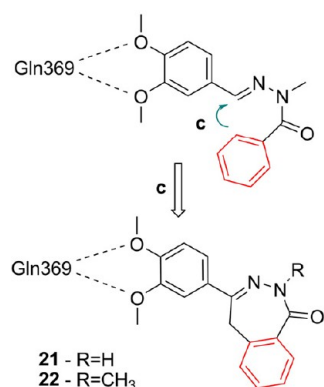**Figure 6.** Design of conformationally constrained derivatives **19** and **20**.

Figure 7. Design of conformationally restricted derivatives **21** and **22**.

The conformationally restricted compounds (**19**−**22**) were screened for their PDE4i activity, as previously described. The results are shown in Table 10 and reveal that only the quinazoline **19** (IC$_{50}$ = 190 nM) was as potent as the prototype **8a** (IC$_{50}$ = 140 nM), suggesting that group 1 could represent the actual bioactive conformation. The lowest activity for **20**

Table 10. PDE4 and TNF-α Inhibition of NAH-Mimetic Heterocyclic Compounds

	PDE4		
compds	% inhib[a]	IC$_{50}$[b] (μM)	TNF-α EC$_{50}$[b] (μM)
8a	97.1	0.14	1.75 ± 0.82
19	98.0	0.19	1.30 ± 0.17
20	81.2	4.1	c
21	78.8	5.2	14% at 10 μM
22	76.5	7.3	20% at 10 μM

[a]Percent inhibition of the PDE4 activity after incubation with the target compound at a drug concentration of 10 μM. [b]The IC$_{50}$ and EC$_{50}$ were calculated by nonlinear regression and represents the mean value of three measurements; the experimental error is approximately 15%. [c]Not determined.

(IC$_{50}$ = 4.1 μM), which was also designed from group 1, could be attributed to steric hindrance introduced by the indazole ring in the catalytic site.

Because of the similar *in vitro* pharmacological profile between **8a** and **19**, we investigated the *in vivo* pharmacological profile for this new quinazoline derivative (Table 11 and Figure 8). As shown in Table 11, LPS stimulation of A/J mice yielded a significant increase in total leucocyte number detected in BAL fluid samples 18 h postchallenge. This elevation was marked by a significant increase in the number of neutrophils. These changes were clearly sensitive to treatment with **19** (100 μmol/kg). However, **8a** inhibited the increase in numbers of total leukocyte and neutrophils by 62% and 67%, respectively, while **19** was less effective and displayed inhibition of only 47% and 49%, respectively. Additionally, LPS increased the TNF-α and IL-6 levels approximately 4-fold, 18 h after challenge, and this increase was inhibited by treatment with **19** by 70% and 86%, respectively. This inhibition was similar to the response observed with **8a** treatment (Table 6).

LPS exacerbated airway resistance and elastance lung response to inhaled methacholine (3−27 mg/mL) compared with control mice challenged with saline (Figure 8A,B, respectively). Figure 8 also shows that treatment with **19** inhibited airway resistance and elastance in mice subjected to LPS challenge by 82% and 66%, respectively (AUC), while treatment with **8a** inhibited by 56% and 64%, respectively (AUC). These results suggest that molecular restriction performed in **19** can serve as a tool for further development of new PDE4 inhibitors with relevant *in vivo* activities.

■ CONCLUSION

This study described a novel pharmacological profile for *N*-methyl-NAH derivatives. When this important chemotype was flanked by two substituted aromatic ring systems (Ar$_1$ and Ar$_2$), it provided a novel series of PDE inhibitors. The selectivity for different PDE isoforms was driven by the following specific substituent effects: (i) The N-methylation and substitution at Ar$_2$ was critical. In particular, the presence of methoxy groups in both *meta* and *para* positions oriented the selective inhibition toward PDE4 (submicromolar). (ii) Substitution at Ar$_1$ increased potency toward PDE4 (e.g., compound **8g**), increased the selectivity profile toward other isoenzymes (e.g., compound **8b**), or completely reoriented the selectivity profile to other PDE subtypes (e.g., compound **8d**). The SAR analysis highlighted the most effective compounds, which displayed both *in vitro* and *in vivo* anti-TNF-α properties.

Based on both the conformational analysis of *N*-methyl-NAH derivatives and the 3D molecular docking studies showing the prototypical PDE4 inhibitor zardaverine in the active site of PDE4, novel heterocyclic NAH-mimetic compounds were designed, synthesized, and tested *in vitro*. The quinazolinone derivative (**19**) appeared as a conformationally restricted NAH mimetic, showing similar effects of both PDE4 inhibition and anti-TNF-α properties, when compared with the corresponding free rotating NAH derivative **8a**.

Our working hypothesis was very efficient because it started with rapid identification of a valuable hit (**8a**) originated from a versatile chemical library (NAHs), followed by rational design of a novel class of heterocyclic NAH-mimetics (**19** as representative) with potent **in vitro** and presenting oral activity.

Table 11. *In Vivo* Protective Activity of 19 (100 μmol/kg, 32 mg/kg) on LPS-Induced Inflammation Pulmonary Models in Mice

| stimulus | treatment | TNF-α | | IL-6 | | total leukocytes[a] | neutrophils[a] |
		pg/mg lung[a]	%[b]	pg/mg lung[a]	%[b]		
saline	vehicle	4.3 ± 1.1		7.1 ± 1.2		70.3 ± 6.9	1.4 ± 0.8
LPS	vehicle	15.9 ± 1.3[c]		33.0 ± 2.1[c]		660.4 ± 61.3[c]	547.2 ± 58.5[c]
	+ 19	7.9 ± 1.1[d]	70	10.7 ± 1.6[d]	86	378.1 ± 24.3[d]	279.0 ± 14.5[d]

[a]Values represent the mean ± SEM (n = 5−7 mice per group) of LPS-stimulated TNF-α and IL-6 release in lung tissue and total leukocyte and neutrophils numbers ($\times 10^3$) in recovered BAL fluid at 100 μmol/kg (vo). [b]% inhibition of LPS-stimulated TNF-α and IL-6 release in lung tissue at 100 μmol/kg (vo) of test compounds. [c]$P < 0.05$ compared with non-LPS-challenged mice (group saline). [d]$P < 0.05$ compared with LPS-challenged mice orally gavaged with vehicle (group LPS).
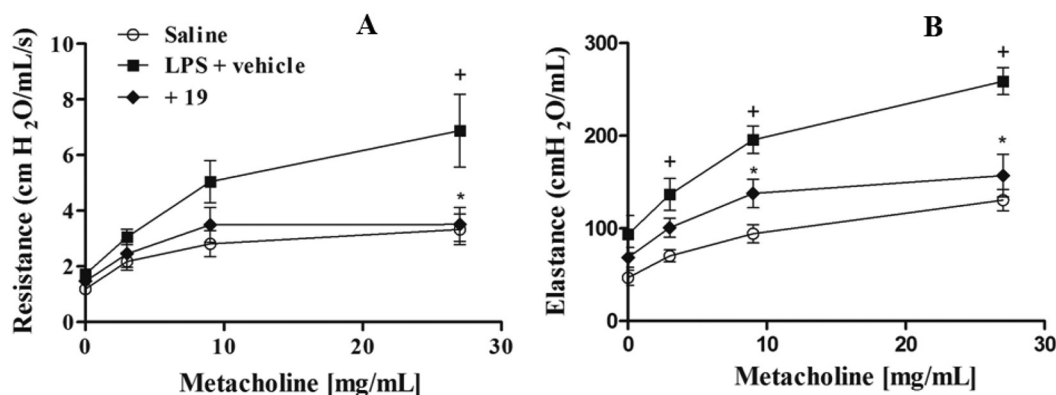

Figure 8. Effect of **19** (100 μmol/kg 32 mg/kg,) on methacholine-induced increases in lung resistance (a) and lung elastance (b) in A/J mice challenged with LPS. Values are mean ± SEM from four to five mice. +$P < 0.05$ compared with sham-challenged mice (○). *$P < 0.05$ compared with LPS-challenged mice orally gavaged with vehicle (■).

■ EXPERIMENTAL SECTION

Synthesis and Characterization of Compounds. *General.* Melting points were determined with a Quimis 340 apparatus and are uncorrected. ^{1}H NMR spectra were determined in deuterated chloroform or dimethyl sulfoxide containing ca. 1% tetramethylsilane as an internal standard, using a Bruker DPX-200 at 200 MHz and a Bruker Avance-400 at 400 MHz. ^{13}C NMR spectra were determined in the same spectrometers at 50 and 100 MHz, respectively, employing the same solvents. IR spectra (cm^{-1}) were taken on an ABB FTLA2000-100 spectrometer in KBr discs. The progress of all reactions was monitored by thin layer chromatography, which was performed on 2.0 × 6.0 cm^2 aluminum sheets precoated with silica gel 60 (HF-254, Merck) to a thickness of 0.25 mm. The developed chromatograms were viewed under ultraviolet light (254−366 nm) and treated with iodine vapor. Reagents and solvents were purchased from commercial suppliers and used as received. Analytical HPLC was used for compound purity determinations using Shimadzu LC-20AD with a SHIM-PACK CLC-ODS analytical column (4.6 mm × 250 mm) or Kromasil 100-5C18 (4.6 mm × 250 mm) and a Shimadzu SPD-M20A detector at 254 nm wavelength. The solvent system used for HPLC analyses was acetonitrile: water = 70:30, with or without of 0.1% trifluoroacetic acid. The isocratic HPLC mode was used, and the flow rate was 1.0 mL/min. The purity of compounds was found to be greater than 95%. Microanalyses were carried out using a Thermo Scientific Flash EA 1112 series CHN-analyzer.

General Procedure for the Preparation of NAH Series 5 and 7. To a solution of hydrazide derivative **11a−g** (0.83 mmol), prepared as described previously,[40,42] in absolute ethanol (7 mL) containing one drop of 37% hydrochloric acid was added 0.87 mmol of the corresponding aromatic aldehyde derivative. The mixture was stirred at room temperature for 1.5 h, until extensive precipitation was seen. Next, the solvent was partially concentrated at reduced pressure, and the resulting mixture was poured into an ice/water mixture. After neutralization with 10% aqueous sodium bicarbonate solution, the precipitate formed was filtered out and dried under vacuum to give the desired NAH derivatives **5a−g** and **7a−g**.

(E)-N′-Benzylidene-3,4-dimethoxybenzohydrazide (5a). The title compound was obtained in 85% yield, by condensing **11a** with benzaldehyde, as a powder with mp 145−146 °C. ^{1}H NMR (200 MHz, DMSO-d_6) δ 11.74 (s, 1H), 8.45 (s, 1H), 7.72 (d, 2H, J = 4.0 Hz), 7.57 (d, 2H, J = 8.4 Hz), 7.50−7.43 (m, 3H), 7.08 (d, 2H, J = 8.4 Hz), 3.83 (s, 6H). ^{13}C NMR (50 MHz, DMSO-d_6) δ 162.8, 151.9, 148.5, 147.4, 134.5, 134.5, 130.0, 128.9, 127.1, 125.5, 121.1, 111.1, 55.7. IR (KBr) 3564, 3225, 1655, 1601, 1275, 1020. MS m/z [M$^+$] 284 (M$^+$, 5%), 181 (33%), 165 (100%), 103 (11%), 137 (7%). Anal. Calcd for C$_{16}$H$_{16}$N$_2$O$_3$: C, 67.59; H, 5.67; N, 9.85. Found: C, 67.61; H, 5.69; N, 9.69.

(E)-N′-(3,4-Dimethoxybenzylidene)-3,4-dimethoxybenzohydrazide (5b). The title compound was obtained in 82% yield, by condensing **11a** with 3,4-dimethoxybenzaldehyde, as a powder with mp 198−199 °C. ^{1}H NMR (200 MHz, DMSO-d_6) δ 11.65 (s, 1H), 8.35 (s, 1H), 7.55 (d, 1H, J = 8.5 Hz), 7.48 (s, 1H), 7.40 (s, 1H), 7.17 (d, 1H, J = 8.5 Hz), 7.06 (d, 1H, J = 8.4 Hz), 7.01 (d, 1H, J = 8.5 Hz), 3.80 (s, 6H). ^{13}C NMR (50 MHz, DMSO-d_6) δ 162.9, 151.9, 150.9, 149.3, 148.5, 147.9, 127.3, 125.6, 122.1, 121.2, 111.6, 111.2, 111.0, 108.5, 55.7, 55.8. IR (KBr) 3236, 1647, 1601, 1269. MS m/z [M$^+$] 344 (M$^+$, 5%), 181 (33%), 165 (100%), 163 (9%), 137 (4%). Anal. Calcd for C$_{18}$H$_{20}$N$_2$O$_5$: C, 62.78; H, 5.85; N, 8.13. Found: C, 62.56; H, 5.90; N, 8.04.

(E)-N′-(Benzo[d][1,3]dioxol-5-ylmethylene)-3,4-dimethoxybenzohydrazide (5c). The title compound was obtained in 86% yield, by condensing **11a** with piperonal, as a powder with mp 171−172 °C. ^{1}H NMR (200 MHz, DMSO-d_6) δ 11.64 (s, 1H), 8.34 (s, 1H), 7.54 (d, 1H, J = 8.4 Hz), 7.46 (s, 1H), 7.32 (s, 1H), 7.15 (d, 1H, J = 8.0 Hz), 7.06 (d, 1H, J = 8.4 Hz), 6.97 (d, 1H, J = 8.0 Hz), 6.07 (s, 2H), 3.80 (s, 6H). ^{13}C NMR (50 MHz, DMSO-d_6) δ 162.9, 151.9, 149.2, 148.5, 148.2, 147.4, 128.9, 125.6, 123.5, 121.2, 111.2, 111.0, 108.6, 105.3, 101.7, 55.7, 55.8. IR (KBr) 3440, 3227, 1641, 1599, 1261, 1038. MS m/z [M$^+$] 328 (M$^+$, 5%), 207 (5%), 181 (33%), 165 (100%), 147 (6%), 146 (11%), 137 (4%). Anal. Calcd for C$_{17}$H$_{16}$N$_2$O$_5$: C, 62.19; H, 4.91; N, 8.53. Found: C, 61.84; H, 4.99; N, 8,38.

(E)-N′-(4-Chlorobenzylidene)-3,4-dimethoxybenzohydrazide (5d). The title compound was obtained in 96% yield, by condensing

11a with 4-chlorobenzaldehyde, as a powder with mp 195−196 °C. ^{1}H NMR (200 MHz, DMSO-d_6) δ 11.76 (s, 1H), 8.45 (s, 1H), 7.74 (d, 2H, J = 8.1 Hz), 7.59−7.49 (m, 4H), 7.08 (d, 1H, J = 8.4 Hz), 3.84 (s, 6H). ^{13}C NMR (50 MHz, DMSO-d_6) δ 162.6, 151.8, 148.4, 145.9, 134.4, 133.4, 128.9, 128.9, 128.6, 125.4, 121.1, 111.0, 55.6. IR (KBr) 3442, 3221, 1649, 1599, 1269, 1016. MS m/z [M$^+$] 320 (M$^+$, 1%), 318 (M$^+$, 3%), 181 (22%), 165 (100%), 139 (4%), 137 (14%). Anal. Calcd for $C_{16}H_{15}ClN_2O_3$: C, 60.29; H, 4.74; N, 8.79. Found: C, 60.33; H, 4.71; N, 8.69.

(E)-N′-(4-Methoxybenzylidene)-3,4-dimethoxybenzohydrazide (5e). The title compound was obtained in 97% yield, by condensing **11a** with 4-methoxybenzaldehyde, as a powder with mp 173−174 °C. ^{1}H NMR (200 MHz, DMSO-d_6) δ 11.58 (s, 1H), 8.40 (s, 1H), 7.67 (d, 2H, J = 8.5 Hz), 7.56 (d, 1H, J = 8,0 Hz), 7.49 (s, 1H), 7.10−7.00 (m, 3H), 3.83 (s, 6H), 3.80 (s, 3H). ^{13}C NMR (50 MHz, DMSO-d_6) δ 162.5, 160.8, 151.7, 148.4, 147.2, 128.6, 127.0, 125.6, 120.9, 114.4, 111.0, 55.6, 55.3. IR (KBr) 3245, 1647, 1609, 1256, 1020. MS m/z [M$^+$] 314 (M$^+$, 3%), 181 (32%), 165 (100%), 137 (5%), 133 (5%). Anal. Calcd for $C_{17}H_{18}N_2O_4$: C, 64.96; H, 5.77; N, 8.91. Found: C, 64.62; H, 5.81; N, 8.78.

(E)-N′-(4-Hydroxybenzylidene)-3,4-dimethoxybenzohydrazide (5f). The title compound was obtained in 93% yield, by condensing **11a** with 4-hydroxybenzaldehyde, as a powder with mp 225−227 °C. ^{1}H NMR (200 MHz, DMSO-d_6) δ 11.52 (s, 1H), 9.94 (s, 1H), 8.36 (s, 1H), 7.56 (d, 2H, J = 8.5 Hz), 7.54−7.49 (m, 3H), 7.07 (d, H$_6$, J = 8.5 Hz), 6.84 (d, 2H, J = 8.5 Hz), 3.83 (s, 3H). ^{13}C NMR (50 MHz, DMSO-d_6) δ 162.4, 159.4, 151.6, 148.4, 147.7, 128.8, 125.7, 125.5, 120.9, 115.8, 111.0, 55.7, 55.6. IR (KBr) 3278, 3182, 1647, 1603, 1271, 1026. MS m/z [M$^+$] (N,O-CH$_3$ derivatization) 328 (M$^+$, 5%), 195 (11%), 165 (100%), 137 (4%), 133 (7%). Anal. Calcd for $C_{16}H_{16}N_2O_4$: C, 63.99; H, 5.37; N, 9.33. Found: C, 63.80; H, 5.41; N, 9.14.

(E)-3,4-Dimethoxy-N′-((2-methylimidazo[1,2-a]pyridin-3-yl)-methylene)benzohydrazide (5g). The title compound was obtained in 73% yield, by condensing **11a** with 2-methylimidazo[1,2-a]pyridine-3-carbaldehyde, as a powder with mp 235−236 °C. ^{1}H NMR (200 MHz, DMSO-d_6) δ 11.75 (s, 1H), 9.62 (d, 1H, J = 6.7 Hz), 8.82 (s, 1H), 7.70−7.47 (m, 4H), 7.23 (t, 1H, J = 6.7 Hz), 7.09 (d, 1H, J = 8.3 Hz), 3.84 (s, 3H), 3.83 (s, 3H), 2.50 (s, 3H). ^{13}C NMR (50 MHz, DMSO-d_6) δ 162.1, 151.7, 148.4, 147.1, 145.0, 137.5, 128.0, 127.5, 125.4, 120.8, 115.9, 115.8, 114.1, 111.1, 110.8, 55.7, 13.1. IR (KBr) 3421, 3203, 1633, 1612, 1267, 1026. MS m/z [M$^+$] 338 (M$^+$, 3%), 181 (25%), 165 (100%), 157 (3%), 137 (6%). Anal. Calcd for $C_{18}H_{18}N_4O_3$: C, 63.89; H, 5.36; N, 16.56. Found: C, 63.78; H, 5.39; N, 16.51.

(E)-N′-(3,4-Dimethoxybenzylidene)benzohydrazide (7a). The title compound was obtained in 71% yield, by condensing **11b** with 3,4-dimethoxybenzaldehyde, as a powder with mp 171−172 °C. ^{1}H NMR (200 MHz, DMSO-d_6) δ 11.78 (s, 1H), 8.37 (s, 1H), 7.90 (d, 2H, J = 6.7 Hz), 7.59−7.48 (m, 3H), 7.38 (s, 1H), 7.20 (d, 1H, J = 8.2 Hz), 7.02 (d, 1H, J = 8.2 Hz), 3.81 (s, 6H). ^{13}C NMR (50 MHz, DMSO-d_6) δ 163.2, 150.9, 149.2, 148.2, 133.6, 131.8, 128.6, 127.7, 127.1, 122.0, 111.6, 108.3, 55.6. IR (KBr) 3225, 1645, 1599, 1267, 1026. MS m/z [M$^+$] 284 (M$^+$, 4%), 163 (5%), 121 (30%), 105 (100%). Anal. Calcd for $C_{16}H_{16}N_2O_3$: C, 67.59; H, 5.67; N, 9.85. Found: C, 67.51; H, 5.68; N, 9.88.

(E)-N′-(3,4-Dimethoxybenzylidene)benzo[d][1,3]dioxole-5-carbohydrazide (7b). The title compound was obtained in 83% yield, by condensing **11c** with 3,4-dimethoxybenzaldehyde, as a powder with mp 182−183 °C. ^{1}H NMR (200 MHz, DMSO-d_6) δ 11.65 (s, 1H), 8.31 (s,1H), 7.48 (d, 1H, J = 8.2 Hz), 7.41 (s, 2H), 7.17 (d, 1H, J = 8.2 Hz), 7.04−6.97 (m, 2H), 6.09 (s, 2H), 3.79 (s, 6H). ^{13}C NMR (50 MHz, DMSO-d_6) δ 162.8, 151.0, 150.5, 149.3, 148.2, 147.7, 127.4, 127.3, 123.1, 122.4, 111.7, 108.5, 108.4, 107.8, 102.1, 55.9, 55.8. IR (KBr) 3230, 1651, 1599, 1267, 1034. MS m/z [M$^+$] 328 (M$^+$, 7%), 165 (32%), 163 (15%), 149 (100%), 121 (13%). Anal. Calcd for $C_{17}H_{16}N_2O_5$: C, 62.19; H, 4.91; N, 8.53. Found: C, 62.16; H, 4.94; N, 8.43.

(E)-4-Chloro-N′-(3,4-dimethoxybenzylidene)benzohydrazide (7c). The title compound was obtained in 73% yield, by condensing **11d**

with 3,4-dimethoxybenzaldehyde, as a powder with mp 159−160 °C. ^{1}H NMR (200 MHz, DMSO-d_6) δ 11.16 (s, 1H), 8.36 (s, 1H), 7.92 (d, 2H, J = 8.4 Hz), 7.59 (d, 2H, J = 8.4 Hz), 7.37 (s, 1H), 7.20 (d, 1H, J = 8.2 Hz), 7.01 (d, 1H, J = 8.2 Hz), 3.80 (s, 6H). ^{13}C NMR (50 MHz, DMSO-d_6) δ 162.1, 150.9, 149.2, 148.5, 136.6, 132.1, 129.6, 128.7, 126.9, 122.2, 111.6, 108.4, 55.6. IR (KBr) 3423, 3226, 1640, 1605, 1269, 1026. MS m/z [M$^+$] 320 (M$^+$, 3%), 318 (M$^+$, 8%), 163 (100%), 148 (20%), 139 (60%), 111 (22%). Anal. Calcd for $C_{16}H_{15}ClN_2O_3$: C, 60.29; H, 4.74; N, 8.79. Found: C, 60.20; H, 4.72; N, 8.81.

(E)-N′-(3,4-Dimethoxybenzylidene)-4-methoxybenzohydrazide (7d). The title compound was obtained in 72% yield, by condensing **11e** with 3,4-dimethoxybenzaldehyde, as a powder with mp 169−170 °C. ^{1}H NMR (200 MHz, DMSO-d_6) δ 11.61 (s, 1H), 8.36 (s, 1H), 7.90 (d, 2H, J = 8.7 Hz), 7.33 (s, 1H), 7.18 (d, 2H, J = 8.3 Hz), 7.04 (d, 2H, J = 8.7 Hz), 7.01 (d, 2H, J = 8.3 Hz), 3.82 (s, 9H). ^{13}C NMR (50 MHz, DMSO-d_6) δ 162.4, 161.9, 150.6, 149.1, 147.4, 129.4, 127.1, 125.6, 121.6, 113.6, 111.5, 108.2, 55.4. IR (KBr) 3443, 3225, 1645, 1605, 1252, 1022. MS m/z [M$^+$] 314 (M$^+$, 5%), 163 (22%), 151 (25%), 135 (100%), 107 (7%). Anal. Calcd for $C_{17}H_{18}N_2O_4$: C, 64.96; H, 5.77; N, 8.91. Found: C, 64.83; H, 5.79; N, 8,77.

(E)-N′-(3,4-Dimethoxybenzylidene)-4-hydroxybenzohydrazide (7g). The title compound was obtained in 61% yield, by condensing **11h** with 3,4-dimethoxybenzaldehyde, as a powder with mp 234−235 °C. ^{1}H NMR (200 MHz, DMSO-d_6) δ 11.53 (s, 1H), 10.10 (s, 1H), 8.36 (s, 1H), 7.80 (d, 2H, J = 8.5 Hz), 7.32 (s, 1H), 7.17 (d, 1H, J = 8.3 Hz), 7.01 (d, 1H, J = 8.3 Hz), 6.86 (d, 2H, J = 8.5 Hz), 3.80 (s, 6H). ^{13}C NMR (50 MHz, DMSO-d_6) δ 162.7, 160.6, 150.6, 149.1, 147.1, 129.6, 127.3, 124.0, 121.6, 115.0, 111.5, 108.2, 55.5. IR (KBr) 3271, 3064, 1651, 1605, 1261, 1016. MS m/z [M$^+$] (N,O-CH$_3$ derivatization) 328 (M$^+$, 7%), 165 (15%), 163 (7%), 135 (100%), 107 (7%). Anal. Calcd for $C_{16}H_{16}N_2O_4$: C, 63.99; H, 5.37; N, 9.33. Found: C, 63.73; H, 5.32; N, 9,12.

(E)-N′-(3,4-Dimethoxybenzylidene)-2-methylimidazo[1,2-a]-pyridine-3-carbohydrazide (7h). The title compound was obtained in 72% yield, by condensing **11i** with 3,4-dimethoxybenzaldehyde, as a powder with mp 223−225 °C. ^{1}H NMR (200 MHz, DMSO-d_6) δ 11.41 (s, 1H), 8.85 (d, 1H, J = 8.3 Hz), 8.25 (s, 1H), 7.60 (d, 1H, J = 8.5 Hz), 7.41 (dd, 1H, J_{ax} = 7.1 Hz, J_{bx} = 8.5 Hz), 7.28 (s, 1H), 7.18 (d, 1H, J = 8.3 Hz), 7.07−6.99 (m, 2H), 6.86 (d, 1H, J = 8.5 Hz), 3.80 (s, 3H), 3.77 (s, 3H), 2.57 (s, 3H). ^{13}C NMR (50 MHz, DMSO-d_6) δ 50.7, 149.0, 146.3, 145.3, 127.2, 126.9, 126.8, 121.6, 116.2, 115.2, 113.0, 111.5, 108.2, 126.9, 55.6, 15.7. IR (KBr) 3211, 1634, 1601, 1269, 1026. MS m/z (N-methyl derivative) [M$^+$] 352 (M$^+$, 7%), 189 (3%), 163 (6%), 159 (100%), 131 (1%). Anal. Calcd for $C_{18}H_{18}N_4O_3$: C, 63.89; H, 5.36; N, 16.56. Found: C, 63.52; H, 5.30; N, 16.42.

General Procedure for Selective N-Methylation of 5a−e and 7a−f (Compounds 6a−e and 8a−f). The corresponding N-acylhydrazone derivative (1.0 mmol) and potassium carbonate (3.0 mmol) were suspended in 5 mL of acetone. The suspension was thoroughly mixed under vigorous stirring for 5 min, and then methyl iodide (3.0 mmol) was added. The reaction was heated at 50 °C and maintained under stirring for 24 h. Afterward, the reaction was evaporated under reduced pressure; the residual solid was suspended in 2 mL of ethanol and then poured into cold water containing a small amount of sodium bisulfite. Purification was achieved by simple filtration, washing of the crude material (water, petroleum ether), and drying under reduced pressure to afford the desired N-methyl-NAH derivatives **6a−e** and **8a−f**.

(E)-N′-Benzylidene-3,4-dimethoxy-N-methylbenzohydrazide (6a). The title compound was obtained in 87% yield, by N-alkylation of **5a** with methyl iodide, as a powder with mp 99−100 °C. ^{1}H NMR (200 MHz, CDCl$_3$) δ 7.77 (s, 1H), 7.55 (d, 2H, J = 5.6 Hz), 7.47 (d, 2H, J = 8.5 Hz), 7.40−7.33 (m, 4H), 7.08 (d, 1H, J = 8.4 Hz), 3.96 (s, 3H), 3.93 (s, 3H), 3.57 (s, 3H). ^{13}C NMR (50 MHz, CDCl$_3$) δ 170.4, 151.1, 147.8, 139.0, 135.0, 129.7, 128.9, 127.1, 127.0, 124.4, 113.9, 109.8, 56.0, 29.2. IR (KBr) 2960, 2912, 1645, 1601, 1261, 1024. MS m/z [M$^+$] 298 (M$^+$, 6%), 195 (10%), 165 (100%), 137 (5%), 103 (8%). Anal. Calcd for $C_{17}H_{18}N_2O_3$: C, 68.44; H, 6.08; N, 9.39. Found: C, 68.21; H, 6.06; N, 9.21.

(E)-N′-(3,4-Dimethoxybenzylidene)-3,4-dimethoxy-N-methylben-zohydrazide (6b). The title compound was obtained in 91% yield, by N-alkylation of **5b** with methyl iodide, as a powder with mp 115−116 °C. ^{1}H NMR (200 MHz, CDCl$_3$) δ 7.69 (s, 1H), 7.44 (d, 1H, J = 8.3 Hz), 7.38 (s, 1H), 7.15 (s, 1H), 7.06 (d, 1H, J = 8.3 Hz), 6.92−6.81 (m, 2H), 3.96−3.78 (m, 12H), 3.54 (s, 3H). ^{13}C NMR (50 MHz, CDCl$_3$) δ 170.3, 150.9, 150.6, 149.5, 147.8, 138.6, 128.2, 127.6, 124.3, 121.7, 113.9, 110.9, 109.6, 108.2, 56.1, 55.8, 29.0. IR (KBr) 2958, 2918, 1647, 1599, 1269, 1020. MS m/z [M$^+$] 358 (M$^+$, 4%), 195 (12%), 165 (100%), 163 (4%), 137 (5%). Anal. Calcd for C$_{19}$H$_{22}$N$_2$O$_5$: C, 63.67; H, 6.19; N, 7.82. Found: C, 63.52; H, 6.22; N, 7.75.

(E)-N′-(Benzo[d][1,3]dioxol-5-ylmethylene)-3,4-dimethoxy-N-methylbenzohydrazide (6c). The title compound was obtained in 93% yield, by N-alkylation of **5c** with methyl iodide, as a powder with mp 189−190 °C. ^{1}H NMR (200 MHz, CDCl$_3$) δ 7.68 (s, 1H), 7.44 (dd, 1H, Jax = 8.6 Hz, Jbx = 2.1 Hz), 7.38 (d, 1H, J = 2.1 Hz), 7.08 (s, 1H), 6.99 (d, 1H, J = 8.6 Hz), 6.90 (d, 1H, J = 8.6 Hz), 6.79 (d, 1H, J = 8.6 Hz), 3.95 (s, 3H), 3.93 (s, 3H), 3.53 (s, 3H). ^{13}C NMR (50 MHz, CDCl$_3$) δ 170.3, 151.0, 149.1, 148.5, 147.9, 138.8, 129.7, 127.4, 124.3, 123.3, 113.8, 109.8, 108.4, 105.7, 101.5, 56.1, 29.2. IR (KBr) 2966, 2914, 1641, 1601, 1269, 1029. MS m/z [M$^+$] 342 (M$^+$, 3%), 195 (15%), 165 (100%), 147 (13%), 146 (22%), 137 (5%). Anal. Calcd for C$_{18}$H$_{18}$N$_2$O$_5$: C, 63.15; H, 5.30; N, 8.18. Found: C, 62.94; H, 5.31; N, 7.99.

(E)-N′-(4-Chlorobenzylidene)-3,4-dimethoxy-N-methylbenzohydrazide (6d). The title compound was obtained in 97% yield, by N-alkylation of **5d** with methyl iodide, as a powder with mp 109−110 °C. ^{1}H NMR (200 MHz, CDCl$_3$) δ 11.76 (s, 1H), 8.45 (s, 1H), 7.74 (d, 2H, J = 8.1 Hz), 7.59−7.49 (m, 4H), 7.08 (d, 1H, J = 8.4 Hz), 3.84 (s, 6H). ^{13}C NMR (50 MHz, CDCl$_3$) δ 170.5, 151.2, 148.0, 137.6, 135.5, 133.6, 129.2, 128.4, 127.2, 124.4, 113.8, 109.9, 56.1, 29.2. IR (KBr) 2960−2935, 1660, 1601, 1269, 1026. MS m/z [M$^+$] 334 (M$^+$, 1%), 332 (M$^+$, 3%), 195 (6%), 165 (100%), 139 (3%), 137 (13%). Anal. Calcd for C$_{17}$H$_{17}$ClN$_2$O$_3$: C, 61.36; H, 5.15; N, 8.42. Found: C, 61.11; H, 5.15; N, 8.26.

(E)-3,4-Dimethoxy-N′-(4-methoxybenzylidene)-N-methylbenzohydrazide (6e). The title compound was obtained in 98% yield, by N-alkylation of **5e** with methyl iodide, as a powder with mp 57−58 °C. ^{1}H NMR (200 MHz, CDCl$_3$) δ 7.72 (s, 1H), 7.49 (d, 2H, J = 8.3 Hz), 7.45 (dd, 1H, Jax = 8.2 Hz, Jbx = 1.6 Hz), 7.38 (d, 1H, J = 1.6 Hz), 6.90 (d, 1H, J = 8.2 Hz), 6.86 (d, 2H, J = 8.3 Hz), 3.94 (s, 3H), 3.87 (s, 3H), 3.80 (s, 3H), 3.55 (s, 3H). ^{13}C NMR (50 MHz, CDCl$_3$) δ 170.3, 160.9, 151.0, 147.8, 138.9, 128.7, 127.8, 127.5, 124.3, 114.3, 113.9, 109.8, 56.0, 55.5, 29.1. IR (KBr) 2962−2935, 1637, 1609, 1261, 1022. MS m/z [M$^+$] 328 (M$^+$, 3%), 195 (20%), 165 (100%), 137 (5%), 133 (10%). Anal. Calcd for C$_{18}$H$_{20}$N$_2$O$_4$: C, 65.84; H, 6.14; N, 8.53. Found: C, 65.69; H, 6.26; N, 8.23.

(E)-N′-(3,4-Dimethoxybenzylidene)-N-methylbenzohydrazide (8a). The title compound was obtained in 93% yield, by N-alkylation of **7a** with methyl iodide, as a powder with mp 105−106 °C. ^{1}H NMR (200 MHz, CDCl$_3$) δ 7.68 (s, 1H), 7.30 (d, 2H, J = 8.0 Hz), 7.42−7.36 (m, 3H), 7.09 (s, 1H), 7.20 (d, 1H, J = 8.0 Hz), 6.82 (d, 1H, J = 8.0 Hz), 3.88 (s, 3H), 3.74 (s, 3H), 3.55 (s, 3H). ^{13}C NMR (50 MHz, CDCl$_3$) δ 171.0, 150.5, 149.4, 138.5, 135.6, 130.0, 129.8, 128.0, 127.2, 121.8, 110.7, 107.8, 56.0, 55.4, 28.6. IR (KBr) 2956−2914, 1640, 1603, 1269, 1026. MS m/z [M$^+$] 298 (M$^+$, 18%), 293 (12%), 163 (98%), 134 (11%), 105 (100%), 77 (57%). Anal. Calcd for C$_{17}$H$_{18}$N$_2$O$_3$: C, 68.44; H, 6.08; N, 9.39. Found: C, 68.22; H, 6.03; N, 9.23.

(E)-N′-(3,4-Dimethoxybenzylidene)-N-methylbenzo[d][1,3]-dioxole-5-carbohydrazide (8b). The title compound was obtained in 92% yield, by N-alkylation of **7b** with methyl iodide, as a powder with mp 204−205 °C. ^{1}H NMR (200 MHz, CDCl$_3$) δ 7.67 (s, 1H), 7.34 (d, 1H, J = 8.0 Hz), 7.27 (s, 2H), 7.27 (s, 1H), 7.07 (s, 1H), 6.98 (d, 1H, J = 8.0 Hz), 6.83 (d, 1H, J = 8.0 Hz), 6.80 (d, 1H, J = 8.0 Hz), 6.03 (s, 2H), 5.98 (s, 2H), 3.52 (s, 3H). ^{13}C NMR (50 MHz, CDCl$_3$) δ 162.9, 150.3, 148.0, 148.0, 134.4, 130.1, 128.9, 128.9, 127.2, 122.9, 108.1, 107.7, 101.9, 29.2. IR (KBr) 2964−2918, 1647, 1607, 1269/1033. MS m/z [M$^+$] 342 (M$^+$, 6%), 179 (12%), 162 (5%), 149

(100%), 121 (13%). Anal. Calcd for C$_{18}$H$_{18}$N$_2$O$_5$: C, 63.15; H, 5.30; N, 8.18. Found: C, 62.80; H, 5.28; N, 7.99.

(E)-4-Chloro-N′-(3,4-dimethoxybenzylidene)-N-methylbenzohydrazide (8c). The title compound was obtained in 93% yield, by N-alkylation of **7d** with methyl iodide, as a powder with mp 119−120 °C. ^{1}H NMR (200 MHz, DMSO-d$_6$) δ 7.70 (d, 2H, J = 8.5 Hz), 7.68 (s, 1H), 7.40 (d, 2H, J = 8.5 Hz), 7.04 (s, 1H), 7.02 (d, 1H, J = 8.1 Hz), 6.83 (d, 1H, J = 8.1 Hz), 3.93 (s, 3H), 3.78 (s, 3H), 3.53 (s, 6H). ^{13}C NMR (50 MHz, DMSO-d$_6$) δ 170.0, 150.8, 149.5, 139.1, 136.2, 134.1, 131.5, 127.9, 127.5, 121.8, 110.9, 108.0, 56.1, 55.7, 28.7. IR (KBr) 2956−2935, 1657, 1605, 1271, 1053. MS m/z [M$^+$] 334 (M$^+$, 4%), 332 (M$^+$, 12%), 193 (17%), 178 (9%), 163 (100%), 139 (70%), 111 (25%). Anal. Calcd for C$_{17}$H$_{17}$ClN$_2$O$_3$: C, 61.36; H, 5.15; N, 8.42. Found: C, 61.53; H, 5.09; N, 8.25.

(E)-N′-(3,4-Dimethoxybenzylidene)-4-methoxy-N-methylbenzohydrazide (8d). The title compound was obtained in 85% yield, by N-alkylation of **7e** with methyl iodide, as a powder with mp 92−93 °C. ^{1}H NMR (200 MHz, DMSO-d$_6$) δ 7.80 (d, 2H, J = 8.8 Hz), 7.67 (s, 1H), 7.17 (d, 1H, J = 1.7 Hz), 7.03 (dd, 2H, Jax = 8.3 Hz, Jbx = 1.7 Hz), 6.90 (d, 2H, J = 8.7 Hz), 6.83 (d, 1H, J = 8.3 Hz), 3.88 (s, 9H), 3.83 (s, 3H), 3.80 (s, 3H), 3.52 (s, 3H). ^{13}C NMR (50 MHz, DMSO-d$_6$) δ 170.2, 161.3, 150.4, 149.3, 138.2, 132.4, 128.2, 127.4, 121.6, 112.4, 110.7, 108.0, 55.9, 55.6, 55.3, 28.7. IR (KBr) 2956−2916, 1639, 1607, 1267, 1254, 1049, 1026. MS m/z [M$^+$] 328 (M$^+$, 8%), 165 (15%), 163 (6%), 135 (100%), 107 (7%). Anal. Calcd for C$_{18}$H$_{20}$N$_2$O$_4$: C, 65.84; H, 6.14; N, 8.53. Found: C, 65.82; H, 6.04; N, 8.20.

(E)-N′-(3,4-Dimethoxybenzylidene)-3-methoxy-N-methylbenzohydrazide (8e). The title compound was obtained in 75% yield, by N-alkylation of (E)-N′-(3,4-dimethoxybenzylidene)-3-methoxybenzohydrazide with methyl iodide, as a powder with mp 62−63 °C. ^{1}H NMR (200 MHz, DMSO-d$_6$) δ 7.61 (s, 1H), 7.25−7.04 (m, 3H), 6.95 (d, 1H, J = 1.7 Hz), 6.92−6.81 (m, 2H), 6.74 (d, 1H, J = 8.2 Hz), 3.81 (s, 9H), 3.74 (s, 3H), 3.68 (s, 3H), 3.50 (s, 3H). ^{13}C NMR (50 MHz, DMSO-d$_6$) δ 170.6, 156.2, 150.4, 149.2, 137.8, 129.9, 128.2, 127.2, 121.6, 120.1, 110.5, 110.4, 107.4, 55.9, 55.7, 55.5, 28.0. IR (KBr) 2999, 2970, 2935, 2837, 1626, 1603, 1577, 1516, 1269, 1240, 1040, 1030. MS m/z [M$^+$] 328 (M$^+$, 11%), 164 (35%), 135 (100%), 107 (35%), 92 (8%), 77 (22%). Anal. Calcd for C$_{18}$H$_{20}$N$_2$O$_4$: C, 65.84; H, 6.14; N, 8.53. Found: C, 65.78; H, 6.23; N, 8.49.

(E)-N′-(3,4-Dimethoxybenzylidene)-2-methoxy-N-methylbenzohydrazide (8f). The title compound was obtained in 91% yield, by N-alkylation of (E)-N′-(3,4-dimethoxybenzylidene)-2-methoxybenzohydrazide with methyl iodide, as a powder with mp 103−104 °C. ^{1}H NMR (200 MHz, DMSO-d$_6$) δ 7.53 (s, 1H), 7.31−7.20 (m, 2H), 6.93 (d, 1H, J = 7.7 Hz), 6.86−6.87 (m, 3H), 6.69 (d, 1H, J = 8.2 Hz), 3.78 (s, 9H), 3.67 (s, 3H), 3.56 (s, 3H), 3.43 (s, 3H). ^{13}C NMR (50 MHz, DMSO-d$_6$) δ 170.8, 158.7, 150.6, 149.4, 138.6, 136.8, 128.2, 128.0, 122.3, 121.8, 115.9, 115.1, 110.6, 107.8, 55.9, 55.5, 55.3, 28.6. IR (KBr) 3080, 3001, 2945, 2910, 2837, 1668, 1604, 1512, 1261, 1034, 1018. MS m/z [M$^+$] 328 (M$^+$, 8%), 163 (11%), 135 (100%), 92 (9%), 77 (18%). Anal. Calcd for C$_{18}$H$_{20}$N$_2$O$_4$: C, 65.84; H, 6.14; N, 8.53. Found: C, 65.88; H, 6.12; N, 8.28.

General Procedure for the Preparation of N-Methyl-NAH Compounds 6f,g and 8g,h. To a solution of the corresponding N-methyl-hydrazide derivative **16a−c** (0.83 mmol), prepared as described previously,[53] in absolute ethanol (7 mL) containing one drop of 37% hydrochloric acid was added 0.87 mmol of the corresponding aldehyde derivative. The mixture was stirred at room temperature for 1.5 h. Next, the solvent was partially concentrated at reduced pressure, and the resulting mixture was poured into ice. After neutralization with 10% aqueous sodium bicarbonate solution, the precipitate formed was collected by filtration and dried under vacuum to afford the desired N-methyl-NAH derivatives **6f,g** and **8g,h**.

(E)-N′-(4-Hydroxybenzylidene)-3,4-dimethoxy-N-methylbenzohydrazide (6f). The title compound was obtained in 72% yield, by condensing **16a** with 4-hydroxybenzaldehyde, as a powder with mp 164−165 °C. ^{1}H NMR (200 MHz, CDCl$_3$) δ 7.74 (s, 1H), 7.48−7.37 (m, 5H), 6.90 (d, 1H, J = 8.6 Hz), 6.84 (d, 2H, J = 8.6 Hz), 3.83 (s, 3H). ^{13}C NMR (50 MHz, CDCl$_3$) δ 170.8, 158.3, 151.1, 147.8, 140.1,

129.0, 127.2, 127.1, 116.1, 113.9, 109.9, 56.1, 56.0, 29.3. IR (KBr) 3215, 2976−2937, 1649, 1603, 1263, and 1024. MS m/z [M⁺] (O-CH₃ derivatization) 328 (M⁺, 3%), 195 (19%), 165 (100%), 137 (5%), 133 (9%). Anal. Calcd for C₁₇H₁₈N₂O₄: C, 64.96; H, 5.77; N, 8.91. Found: C, 65.01; H, 5.79; N, 8.88.

(E)-3,4-Dimethoxy-N-methyl-N′-((2-methylimidazo[1,2-a]pyridin-3-yl)methylene)benzohydrazide (6g). The title compound was obtained in 78% yield, by condensing **16a** with 2-methylimidazo-[1,2-*a*]pyridine-3-carbaldehyde, as a powder with mp 205−206 °C. ¹H NMR (200 MHz, CDCl₃) δ 8.62 (d, 1H, *J* = 7.2 Hz), 8.01 (s, 1H), 7.51 (d, 1H, *J* = 8.5 Hz), 7.30−7.14 (m, 3H), 6.92 (d, 1H, *J* = 8.5 Hz), 6.51 (t, 1H, *J* = 7.2 Hz), 3.96 (s, 3H), 3.82 (s, 3H), 3.59 (s, 3H), 2.56 (s, 3H). ¹³C NMR (50 MHz, CDCl₃) δ 171.8, 150.6, 148.5, 146.3, 129.8, 128.4, 128.1, 126.5, 122.4, 116.5, 112.9, 112.2, 110.3, 56.3, 56.1, 28.4, 14.0. IR (KBr) 2954−2920, 1647, 1605, 1263, and 1028. MS m/z [M⁺] 352 (M⁺, 13%), 195 (13%), 165 (100%), 137 (5%), 133 (10%). Anal. Calcd for C₁₉H₂₀N₄O₃: C, 64.76; H, 5.72; N, 15.90. Found: C, 64.70; H, 5.73; N, 15.86.

(E)-N′-(3,4-Dimethoxybenzylidene)-4-hydroxy-N-methylbenzohydrazide (8g). The title compound was obtained in 93% yield by condensing **16b** with 3,4-dimethoxybenzaldehyde, as a powder with mp 94−95 °C. ¹H NMR (300 MHz, DMSO) δ 9.84 (s, 1H), 7.88 (s, 1H), 7.60 (d, 2H, *J* = 8.8 Hz), 7.16 (d, 1H, *J* = 1.7 Hz), 7.11 (dd, 2H, *Jax* = 8.2 Hz, *Jbx* = 1.7 Hz), 6.97 (d, 1H, *J* = 8.2 Hz), 6.80 (d, 2H, *J* = 8.8 Hz), 3.77 (s, 3H), 3.68 (s, 3H), 3.43 (s, 3H, N−C*H*₃). ¹³C NMR (75 MHz, DMSO) δ 169.0, 159.3, 150.0, 148.9, 139.1, 132.1, 128.0, 125.5, 121.0, 113.8, 111.6, 108.6, 55.5, 55.1, 28.6. IR (KBr) 3524, 2970−2954, 1641, 1607, 1267, and 1047. MS m/z [M⁺] (O-CH₃ derivatization) 328 (M⁺, 6%), 165 (17%), 163 (7%), 135 (100%), 107 (8%). Anal. Calcd for C₁₇H₁₈N₂O₄: C, 64.96; H, 5.77; N, 8.91. Found: C, 64.55; H, 5.82; N, 8.65.

(E)-N′-(3,4-Dimethoxybenzylidene)-N-2-dimethylimidazo[1,2-a]pyridine-3-carbohydrazide (8h). The title compound was obtained in 75% yield, by condensing **16c** with 3,4-dimethoxybenzaldehyde, as a powder with mp 170−171 °C. ¹H NMR (200 MHz, CDCl₃) δ 8.41 (d, 1H, *J* = 6.9 Hz), 7.77 (s, 1H), 7.55 (d, 1H, *J* = 8.7 Hz), 7.25 (t, 1H, *J* = 7.2 Hz), 7.00 (d, 2H, *J* = 8.5 Hz), 6.92 (s, 1H), 6.83−6.76 (m, 2H), 3.85 (s, 3H), 3.63 (s, 3H), 3.58 (s, 3H), 2.49 (s, 3H). ¹³C NMR (50 MHz, CDCl₃) δ 163.4, 150.8, 149.4, 148.4, 145.9, 139.8, 127.3, 125.9, 121.9, 116.5, 116.3, 112.4, 110.7, 107.5, 55.9, 55.7, 28.9, 15.7. IR (KBr) 2984−2939, 1655, 1605, 1258, and 1036. MS m/z [M⁺] 352 (M⁺, 6%), 189 (2%), 163 (6%), 159 (100%), 131 (1%). Anal. Calcd for C₁₇H₁₈N₂O₄: C, 64.76; H, 5.72; N, 15.90. Found: C, 64.61; H, 5.72; N, 15.93.

Synthesis of Quinazoline Derivative (19). 4-Chloroquinazoline (23). A solution of anthranilic acid **22** (400 mg, 2.92 mmol) and formamidine acetate (380 mg, 3.65 mmol) in EtOH (15 mL) was heated in a sealed microwave tube at 130 °C for 40 min. After evaporation of the solvent under reduced pressure, the residue was partitioned between EtOAc (20 mL) and Na₂CO₃ 5% (20 mL). The organic layer was further washed with brine (2 × 20 mL), dried (Na₂SO₄), and evaporated *in vacuo* to afford the quinazolin-4(3*H*)-one as a white powder in 89% yield. This derivative (340 mg, 2.36 mmol) was subsequently dissolved in POCl₃ (8 mL) and heated at 110 °C for 2 h. After evaporation of POCl₃, the crude residue was partitioned between CH₂Cl₂ and 5% aqueous NaHCO₃ solution. The organic layer was washed with water and brine and dried over Na₂SO₄. The solution was concentrated under reduced pressure to provide crude 4-chloroquinazoline as a brown solid in 86% yield, which was used without any further purification.[89]

4-(1-Methylhydrazinyl)quinazoline (24). 4-Chloroquinazoline **23** (150 mg, 0.91 mmol) was dissolved in CH₂Cl₂ (1 mL) and stirred at room temperature. A methylhydrazine solution (210 mg, 4.56 mmol in 1 mL of CH₂Cl₂) was added dropwise The rate of dropping was regulated so that the temperature of the mixture did not exceed 30 °C. The reaction was stirred at room temperature for 45 min followed by an additional time of 3 h at 0 °C. The solution was then concentrated on a rotary evaporator, and to the crude residue 30 mL of ice was added . The resulting mixture was then left under stirring for 20 min. The obtained precipitate was filtered, and the filtrate was extracted

with EtOAc (3 × 30 mL). The organic phase was dried (Na₂SO₄) and evaporated. The combination of products afforded the desired quinazoline **24** in 96% yield.[90]

(E)-4-(2-(3,4-Dimethoxybenzylidene)-1-methylhydrazinyl)-quinazoline (19). To a solution of methylhydrazide **24** (120 mg, 0.69 mmol) in absolute ethanol (3 mL) containing one drop of 37% hydrochloric acid was added 116 mg (0.70 mmol) of the 3,4-dimethoxybenzaldehyde, and the resultant mixture was stirred at room temperature for 10 h. The reaction medium was than neutralized with a cold sodium bicarbonate aqueous solution at 10% (20 mL). The resulting suspension was then extracted with AcOEt (3 × 30 mL). The organic layer was further dried (Na₂SO₄) and evaporated under reduced pressure. Addition of petroleum ether to the crude residue led to the precipitation of the desired product. After filtration of the solid, **19** was obtained in 81% yield as a yellow powder with mp = 146−147 °C. ¹H NMR (400 MHz, CDCl₃) δ 9.19 (dd, 1H, *J* = 8.6, 1.0 Hz), 8.80 (s, 1H), 7.92 (dd, 1H, *J* = 8.4, 1.2 Hz), 7.90 (s, 1H), 7.77 (ddd, 1H, *J* = 8.4, 6.9, 1.0 Hz), 7.48 (ddd, 1H, *J* = 8.6, 6.9, 1.2 Hz), 7.45 (d, 1H, *J* = 2.0 Hz), 7.19 (dd, 1H, *J* = 2.0, 8.3 Hz), 6.93 (d, 1H, *J* = 8.3 Hz), 3.99 (s, 6H), (s, 3H), 3.89 (s, 3H). ¹³C NMR (100 MHz, CDCl₃) δ 160.1, 153.4, 152.5, 150.4, 149.5, 139.0, 132.5, 129.2, 128.4, 128.2, 125.2, 121.5, 117.2, 110.9, 107.8, 56.0, 31.7. IR (KBr) 2997, 2916, 2839, 1603, 1566, 1492, 1267, 1045, 1024. MS m/z [M⁺] 322 (M⁺, 21%), 185 (100%), 158 (31%), 130 (29%). Anal. Calcd for C₁₈H₁₈N₄O₂: C, 67.07; H, 5.63; N, 17.38. Found: C, 66.94; H, 5.55; N, 17.03.

Synthesis of Indazole Derivative (20). 3-Iodo-1H-indazole (26). To a solution of indazole **25** (1.5 g, 12.70 mmol) in DMF (30 mL) was added molecular iodine (6.4 g, 25.40 mmol) and potassium hydroxide (2.7 g, 47.61 mmol) at room temperature. After 1 h, the mixture was poured onto a 10% aqueous NaHCO₃ solution (10 mL). The resulting aqueous layer was than extracted with ethyl ether (3 × 10 mL). The organic phase was dried over Na₂SO₄ and evaporated under reduced pressure to afford **26** as a yellow solid in 88% yield.[91]

(3-(3,4-Dimethoxyphenyl)-1H-indazol-1-yl)(phenyl)methanone (20). A suspension of **26** (500 mg, 2.05 mmol), sodium carbonate (521 mg, 4.92 mmol), Pd(PPh₃)₄ (47 mg, 0.04 mmol), and 3,4-dimethoxyphenylboronic acid (447 mg, 2.46 mmol) in a 3:1 mixture of DME/H₂O (15 mL) was mixed in a process vial and flushed with argon for 2 min. The reaction mixture was then capped properly and thereafter microwave heated to 155 °C for 30 min. The mixture was cooled, and the suspension was concentrated to dryness under reduced pressure. The residue was partitioned between EtOAc (30 mL) and water (2 × 20 mL). The organic layer was evaporated, and the obtained solid was washed with ethyl ether giving **27** (64%), which was used in the next step without any further purification. Compound **27** (240 mg, 0.94 mmol) was dissolved in 10 mL of pyridine and stirred for 15 min at room temperature. Benzoylchloride (159 mg, 1.13 mmol) was then added dropwise, and the resulting mixture was stirred at room temperature for 8 h. The pyridine was evaporated under reduced pressure, and the residue was partitioned between EtOAc (30 mL), 1% aqueous HCl (10 mL), and water (2 × 20 mL). The organic phase was evaporated, and the obtained crude residue was purified by column chromatography over silica gel (using EtOAc/heptane 1:3 as eluant) to afford **20** as a white solid in 74% yield. Mp =143−144 °C. ¹H NMR (400 MHz, CDCl₃) δ 8.67 (d, 1H, *J* = 8.5 Hz), 8.20 (d, 2H, *J* = 8.0 Hz), 8.05 (d, 1H, *J* = 8.0 Hz), 7.67 (ddd, 1H, *J* = 8.41, 7.15, 1.0 Hz), 7.64−7.46 (m, 6H), 7.06 (d, 1H, *J* = 8.5 Hz), 3.97 (s, 6H). ¹³C NMR (100 MHz, CDCl₃) δ 168.2, 150.4, 150.1, 149.4, 141.8, 133.5, 132.2, 131.4, 129.4, 127.8, 125.1, 124.6, 121.3, 121.1, 116.4, 111.3, 111.1, 56.1, 56.0. IR (KBr) 2989, 2962, 2933, 2833, 1685, 1604, 1489, 1371, 1255, 1232, 1026, 999. MS m/z [M⁺] 358 (M⁺, 22%), 105 (100%), 77 (31%). Anal. Calcd for C₂₂H₁₈N₂O₃: C, 73.73; H, 5.06; N, 7.82. Found: C, 73.59; H, 5.16; N, 7.69.

Synthesis of Benzodiazepinone Derivatives (21 and 22). Methyl 2-[(3,4-Dimethoxyphenyl)ethynyl]benzoate (29). To a solution of **28** (500 mg, 2.15 mmol) in dry THF (14 mL) under argon were added 4-bromo-1,2-dimethoxybenzene (934 mg, 4.30 mmol), PPh₃ (158 mg, 0.60 mmol), CuI (41 mg, 0.22 mmol), and piperidine (1832 mg, 21.52 mmol), and the reaction mixture was purged with argon for 15 min. Then K₂CO₃ (654 mg, 4.73 mmol) and Pd(PPh₃)₂Cl₂ (60 mg, 0.09

mmol) were added, and the resulting suspension was heated to reflux. MeOH (2 mL) was added dropwise to this resulting mixture, which was heated for 15 min. The reaction was then cooled at room temperature and diluted with MeOH (10 mL). The mixture was filtered on Celite and concentrated under reduced pressure. The obtained crude oil was purified by column chromatography on silica gel (EtOAc 10% to 25% in heptane) to afford **29** as a brown oil in 85% yield. ^{1}H NMR (400 MHz, CDCl$_3$) δ 7.97 (d, 1H, J = 7.8 Hz), 7.63 (d, 1H, J = 7.8 Hz), 7.48 (dd, 1H, J = 7.5, 7.5 Hz), 7.35 (dd, 1H, J = 7.5, 7.5 Hz), 7.19 (d, 1H, J = 8.1 Hz), 7.08 (s, 1H), 6.85 (d, 1H, J = 8.1 Hz), 3.96 (s, 3H), 3.91 (s, 3H), 3.90 (s, 3H). ^{13}C NMR (100 MHz, CDCl$_3$) δ 165.8, 149.3, 148.2, 133.2, 131.2, 131.0, 129.9, 127.0, 124.7, 123.5, 114.9, 113.8, 110.6, 94.3, 86.6, 55.2, 55.2, 51.4. IR (KBr) 2924, 2852, 2360, 2341, 2206, 1727, 1593, 1513, 1248, 1133, 1078, 1024, 759, 699, 527.

3-(3,4-Dimethoxyphenyl)isocoumarin (30). A solution of **29** (550 mg, 1.86 mmol) in trifluoroacetic acid (2 mL) was stirred for 1 h at room temperature and concentrated under reduced pressure. The residue was partitioned between EtOAc (20 mL) and water (20 mL). The organic layer was further washed with brine (2 × 20 mL), dried (Na$_2$SO$_4$), evaporated *in vacuo*, and subsequently purified by column chromatography on silica gel (AcOEt 30% to 50% in heptane) to afford **30** as a white powder in 91% yield, mp = 110−112 °C. ^{1}H NMR (CDCl$_3$, 400 MHz) δ 8.21 (d, 1H, J = 7.8 Hz), 7.66 (ddd, 1H, J = 1.0, 7.8, 8.3 Hz), 7.40 (ddd, 3H, J = 2.0, 8.3, 8.6 Hz), 7.30 (d, 1H, J = 2.0 Hz), 6.86 (d, 1H, J = 8.6 Hz), 6.82 (s, 1H), 3.92 (s, 3H), 3.88 (s, 3H). ^{13}C NMR (CDCl$_3$, 100 MHz) δ 163.9, 153.9, 151.1, 149.5, 138.4, 135.6, 130.0, 128.3, 126.2, 124.9, 120.0, 118.9, 111.6, 108.5, 101.3, 56.4, 56.3. IR (KBr) 2932, 2836, 2352, 1722, 1631, 1600, 1512, 1463, 1262, 1215, 1169, 1142, 1070, 808, 756, 537.

(E)-4-(3,4-Dimethoxyphenyl)-2,5-dihydro-1H-benzo[d][1,2]-diazepin-1-one (21). Within a flask was dissolved the isocoumarin **30** (100 mg, 0.35 mmol) in 5 mL of *n*-BuOH. Then was added hydrazine hydrate (44 mg, 0.89 mmol), and the mixture was heated to 100 °C for 5 h. At the end of reaction, the solvent was evaporated at reduced pressure to half of initial volume, and the residual solution was taken to an ice bath. After 6 h, the precipitate formed was filtered under vacuum on Büchner funnel furnishing the benzodiazepine **21** in 87% yield, as a solid with mp = 206−207 °C. ^{1}H NMR (CDCl$_3$, 400 MHz) δ 8.89 (s, 1H), 7.96 (d, 1H, J = 8.6 Hz), 7.45 (t, 1H, J = 7.3 Hz), 7.34 (m, 3H), 7.21 (m, 2H), 6.82 (d, 1H, J = 8.0 Hz), 3.97 (s, 2H), 3.84 (s, 3H), 3.83 (s, 3H). ^{13}C NMR (CDCl$_3$, 100 MHz) δ 167.8, 160.1, 151.4, 149.3, 137.3, 133.4, 131.6, 130.9, 127.8, 127.7, 127.1, 120.3, 110.5, 109.5, 56.0, 35.3. IR (KBr) 3437, 3275, 3190, 3065, 2914, 1657, 1601, 1517, 1425, 1275, 1022. MS *m/z* [M$^+$] 296 (M$^+$, 91%), 267 (100%), 252 (16%), 165 (20%). Anal. Calcd for C$_{17}$H$_{16}$N$_2$O$_3$: C, 68.91; H, 5.44; N, 9.45. Found: C, 68.90; H, 5.49; N, 9.33.

(E)-4-(3,4-Dimethoxyphenyl)-2-methyl-2,5-dihydro-1H-benzo[d]-[1,2]diazepin-1-one (22). To a solution of isocoumarin **30** (100 mg, 0.35 mmol) in 5 mL of *n*-BuOH was added methylhydrazine (41 mg, 0.89 mmol), and the resulting mixture was heated to 100 °C for 5 h. At the end of reaction, the volatiles were evaporated at reduced pressure to half of initial volume, and the residual solution was taken to an ice bath. After 1 h, the precipitate was filtered under vacuum on Büchner funnel furnishing the benzodiazepine **22** in 82% yield, as a solid with mp = 147−149 °C. ^{1}H NMR (CDCl$_3$, 400 MHz) δ 7.91 (d, 1H, J = 7.8 Hz), 7.34 (m, 4H), 7.17 (m, 2H), 6.82 (d, 1H, J = 8.3 Hz), 3.89 (s, 2H), 3.85 (s, 6H), 3.57 (s, 3H). ^{13}C NMR (CDCl$_3$, 100 MHz) δ 166.1, 160.9, 151.4, 149.3, 137.5, 132.4, 130.8, 128.9, 127.6, 126.3, 120.4, 110.5, 109.5, 56.0, 39.2, 35.3. IR (KBr) 3437, 3275, 3190, 3065, 2914, 1657, 1601, 1517, 1425, 1275, 1022. IR (KBr) 2932, 2836, 2352, 1722, 1631, 1600, 1512, 1463, 1262, 1215, 1169, 1142, 1070, 808, 756, 537. MS *m/z* [M$^+$] 310 (M$^+$, 88%), 281 (100%), 266 (12%). Anal. Calcd for C$_{18}$H$_{18}$N$_2$O$_3$: C, 69.66; H, 5.85; N, 9.03. Found: C, 69.65; H, 5.87; N, 8.99.

Pharmacological Evaluation. *PDE Inhibition.* PDE4 was isolated from the media layer of bovine aorta according to a modification of the previously reported method.[56] PDE activities were measured by the two-step assay previously described[58] at a [^{3}H]-cAMP or [^{3}H]-cGMP concentration of 1 μM substrate in a buffer solution of 50 mM of Tris-HCl, at pH 7.5, containing 2 mM of magnesium acetate and 1 mg mL^{-1} of BSA. PDE4 was assayed at 1 μM cAMP, 1 mM EGTA. To prevent the influence of reciprocal cross-contamination between PDE3 and PDE4, the studies were always carried out in the presence of 50 μM cGMP for PDE4. PDE1, PDE3, and PDE5 were isolated by anion-exchange chromatography from bovine aortic smooth muscle cytosolic fraction as previously described.[56] PDE2 was isolated from human platelets.[57] Purified PDEs were stored as aliquots at −80 °C until use. PDE inhibitors were dissolved in dimethyl sulfoxide (DMSO) at a final concentration of 1%. At this concentration, DMSO had no significant effect on PDE activity. The concentration of drugs that produced 50% inhibition of substrate hydrolysis (IC$_{50}$) was calculated by nonlinear regression analysis from concentration response curves and included different concentrations of inhibitors. The results represent the mean of three determinations obtained for three different enzymatic preparations. The experimental error is about 15%.

TNF-α Inhibition. Subjects. Healthy donors who had no clinical history were selected for this study. This work was approved by the local ethics committee (CCPPRB d'Alsace no. 1) and carried out according to national guidelines.

Peripheral Blood Mononuclear Cells. PBMCs from healthy subjects were separated as previously described.[92] Briefly, peripheral blood diluted with Hank's balanced salt solution, Ca^{2+} and Mg^{2+} free, containing 100 IU/mL heparin was layered over Histopaque-1077 (Sigma, St. Louis, MO, USA) and centrifuged for 30 min at 400g (20 °C). Cells harvested from the interface were washed three times in HBSS-CMF and resuspended at a final concentration of 2 × 10^6 mL^{-1} in a culture medium. Human PBMCs were incubated with increasing doses of the tested drugs ranging from 10^{-8} to 10^{-5} M, with or without activation by lipopolysaccharide from *Salmonella abortus equi* (Sigma, L'Isled'Abeau Chesnes, France) in 24 well culture plates (Falcon, Poly Labo, Strasbourg, France) for 24 h at 37 °C in a humidified 5% CO$_2$/ 95% air atmosphere. After incubation, supernatants were removed and stored at −80 °C until ELISA. Cell viability was assessed by the Trypan blue exclusion test.

Immunoassays for TNF-α.[93] Culture supernatants were assayed with two-site ELISAs specific for human interleukin: TNFα antibodies (Antibody Solutions, Half Moon Bay, CA, USA). Quantitative evaluation of TNFα secreted by PBMCs was achieved by ELISA using conditions as previously described.[76] Poly(vinyl chloride) plates (Costar, no. 2596) were coated with 50 mL per well of antibodies (15 μg mL^{-1}) and incubated overnight at 4 °C. After the usual wash and nonspecific saturation steps, 25 mL of standard or sample was added to 25 mL of biotinylated monoclonal antibody (2 μg mL^{-1}) for 2 h at room temperature. Following washing steps, 50 mL of peroxidase streptavidin dilution (1:3000 in PBS) was added (1 h at room temperature). A colorimetric reaction (O.D. at 450 nm) using *O*-phenylenediamine as peroxidase substrate was performed ensuing four washing steps. Concentrations (pg/mL) of unknown samples were computed by interpolation with a standard curve run on each plate using four parameters logistics analysis. Standard human recombinant protein, hr-TNFα, was purchased from R&D Systems Europe (Abingdon, U.K.).

In Vivo Assays. Animals. Female A/J mice, 4−6 weeks old, were used in the experiments. All animals were obtained from Oswaldo Cruz Foundation and maintained in the animal-housing facilities at a controlled room temperature (22−25 °C) and a 12 h (6 a.m. to 6 pm) light−dark cycle. Procedures involving the care and use of laboratory animals were examined and approved by the Animal Ethics Committee of the Oswaldo Cruz Foundation (L-0028/06; CEUA-FIOCRUZ, Rio de Janeiro, Brazil).

LPS-Induced Lung Inflammation. Female A/J mice were anesthetized with aerosolized halothane for provocation by nasal instillation with LPS (25 μg/25 μL) or saline (negative control), 18 h before assays. Rolipram (Sigma) and compounds **6b** and **8a−g** were dissolved in 0.2% Tween 80 (vehicle) and dosed orally 1 h before LPS. Cilomilast (Axon MedChem) (1.6 mg) was dissolved in 1 M NaOH (about 80 μL), made up to 600 μL of distilled water, and then neutralized with 1 N HCl. All treatments were performed orally 1 h before LPS challenge.

Invasive Assessment of Respiratory Mechanics. Airway responsiveness was assessed as a change in airway function 18 h after provocation with aerosolized methacholine in a FinePoint R/C Buxcos Platform (Buxco Electronics, Sharon, CT, USA). Mice were anaesthetized with nembutal (60 mg/kg). Neuromuscular activity was blocked with bromide pancuronium (1 mg/kg). Tracheostomized mice were mechanically ventilated and lung function was assessed. The trachea was cannulated and the cannula was connected to a pneumotachograph. Airflow and transpulmonary pressure were recorded using a Buxco pulmonary mechanics processing system (Buxco Electronics, Wilmington, NC, USA). This instrument was used to calculate lung resistance (cm $H_2O/(mL\cdot s)$) and elastance (cm H_2O/mL) in each breath cycle. Analog signals from the computer were digitized using a Buxco analog/digital converter (Buxco Electronics). Mice were allowed to stabilize for 5 min, and increasing concentrations of methacholine (3, 9, and 27 mg/mL) were aerosolized for 5 min each. Baseline pulmonary parameters were assessed with aerosolized phosphate-buffered saline (PBS). Expressed results comprised the mean absolute values of the responses of lung resistance and elastance collected during 5 min after the administration of methacholine aerosol.

Bronchoalveolar Lavage. After evaluation of ARH, mice were killed, and bronchoalveolar lavage (BAL) was performed twice by intratracheal instillation of 800 μL of PBS and EDTA (10 mM). The lavage fluid was centrifuged, and cell pellets were resuspended in PBS, final volume 250 μL. The number of leukocytes in BAL fluid was estimated in a Neubauer chamber. Cytospin slides were prepared from BAL fluid and stained with Giemsa stain. At least 100 cells were counted per slide under light microscopy, and they were differentiated according to standard morphological criteria.

ELISA. ELISA measurement of TNF-α and IL-6 was performed on lung tissue lysates of A/J mice provoked with LPS or saline. Briefly, microwell strips were coated with an anti-TNFα or an anti-IL-6 murine monoclonal antibody (R&D Systems) overnight. Samples were then added to the wells and incubated with the biotinylated antibody (R&D Systems) for 2 h at room temperature. HRP-conjugated streptavidin was applied on samples before signal revelation.

Duration of Anesthesia Induced by the Association of Xylazine and Ketamine. These experiments were done following procedures previously described.[26,62] In distinct animal groups, **8d** or **8g** (30−200 μmol/kg), rolipram (1−50 μmol/kg), or vehicle (0.2% Tween 80) was subcutaneously administered into 8−12-week-old female A/J mice, 30 min prior to an intraperitoneal injection of a mixed solution of xylazine (10 mg/kg) and ketamine (70 mg/kg). The duration of anesthesia (i.e., period in which the animal remained on its back spontaneously) was measured as the end point.

Statistical Analyses. Statistical analyses were carried out with ANOVA followed by the Newman−Keuls−Student test. P40.05 (two-tailed test) was considered significant.

Docking Studies. *General.* All calculations have been performed on a PC running under Linux Red Hat v5.0 workstation. Structural manipulations were performed using Sybyl 7.3.[94]

Preparation of the Ligands. The ligands were built in Spartan '08 (Wavefunction Inc.). After preliminary minimization with the MMFF force field,[95] it was submitted to full-energy minimization with the semiempiric method AM1,[96] also in Spartan '08. A systematic conformational search was performed on the rotatable bonds using default angles. The lowest-energy conformation was selected for further AM1 geometry optimization, and Gasteiger−Hückel charge was assigned for docking studies, as required by the docking software.

Selection of Protein Crystal Structures. Ligand-bound crystallographic structures of PDE4 are available in the Protein Data Bank. The crystal structure of zardaverine bound to human PDE4D was used (PDB ID code 1XOR; resolution 1.54 Å).[85] The active recognition site of the ensemble has been defined as the collection of residues within 8.0 Å of the bound inhibitor and comprised the union of all ligands of the ensemble. All atoms located less than 8.0 Å from any ligand atom were considered, covering the important residues Gln369 and Phe372 and also the Zn^{2+} and Mg^{2+} metal ions. Proteins were prepared for the

docking studies using the Biopolymer module of Sybyl 7.3. Amber F99[86] charges were attributed to the protein atoms.

Next, Biopolymer protein analysis tool was used, in a stepwise process of analysis and correction of geometry parameters. For each structure, the description of an ensemble contains the definition of the protein atoms (via chain identifiers and hetero groups), the resolution of ambiguities in the PDB file (alternate location indicators, etc.), the location of hydrogen atoms at hetero atoms, and the definition of the active site atoms. The assignment of hydrogen positions has been made on the basis of default rules except for the definition of the hydrogen positions inside the histidine side chain. The side chains of lysine and arginine and the carboxylate groups of aspartic and glutamic acid have been modeled in their ionized states. Water molecules contained in the catalytic site of the PDB file have been maintained. The default FlexX scoring function was used to rank order the docked conformational groups, and the best-docked result for each group was then used to analyze the binding interactions.

ASSOCIATED CONTENT

S **Supporting Information**
^{1}H and ^{13}C NMR spectra of all *N*-acylhydrazones, *N*-methyl-*N*-acylhydrazones, and their constrained heterocyclic analogues and the effects of cilomilast in LPS-induced airway hyper-reactivity. This material is available free of charge via the Internet at http://pubs.acs.org.

AUTHOR INFORMATION

Corresponding Author
*Phone: +55-21-2562-6644. Fax: +55-21-2562-6478. E-mail: ejbarreiro@ccsdecania.ufrj.br.

Present Address
‖Departamento de Química, Universidade Federal Rural do Rio de Janeiro, BR-465, Km7, Seropédica, RJ 23890-000, Brazil.

Author Contributions
⊥These authors contributed equally to this work.

Notes
The authors declare no competing financial interest.

ACKNOWLEDGMENTS

ABREVIATIONS USED

NAH, *N*-acylhydrazone; cAMP, cyclic adenosine monophosphate; cGMP, cyclic guanosine monophosphate; IL, interleukin; Gln369, glutamine 369; Phe372, phenylalanine 372; PDE4i, phosphodiesterase 4 inhibition; BAL, bronchoalveolar lavage

REFERENCES

(1) Beavo, J. A. Cyclic nucleotide phosphodiesterases: Functional implications of multiple isoforms. *Physiol. Rev.* **1995**, *75*, 725−748.
(2) Conti, M.; Jin, S. L. The molecular biology of cyclic nucleotide phosphodiesterases. *Prog. Nucleic Acid Res. Mol. Biol.* **1999**, *63*, 1−38.
(3) Houslay, M. D. Adaptation in cyclic AMP signalling processes: A central role for cyclic AMP phosphodiesterases. *Semin. Cell Dev. Biol.* **1998**, *9*, 161−167.
(4) Keravis, T.; Lugnier, C. Cyclic nucleotide phosphodiesterase (PDE) isozymes as targets of the intracellular signalling network: Benefits of PDE inhibitors in various diseases and perspectives for future therapeutic developments. *Br. J. Pharmacol.* **2012**, *165*, 1288−1305.

(5) Francis, S. H.; Turko, I. V.; Corbin, J. D. Cyclic nucleotide phosphodiesterases: Relating structure and function. *Nucleic Acid Res. Mol. Biol.* **2000**, *65*, 1−52.

(6) Manallack, D.; Hughes, R.; Thompson, P. The next generation of phosphodiesterase inhibitors: Structural clues to ligand and substrate selectivity of phosphodiesterases. *J. Med. Chem.* **2005**, *48*, 3449−3462.

(7) Lugnier, C. Cyclic nucleotide phosphodiesterase (PDE) super-family: A new target for the development of specific therapeutic agents. *Pharmacol. Ther.* **2006**, *109*, 366−398.

(8) Menniti, F. S.; Faraci, W. S.; Schmidt, C. J. Phosphodiesterases in the CNS: Targets for drug development. *Nat. Rev. Drug Discovery* **2006**, *5*, 660−670.

(9) Houslay, M. D.; Schafer, P.; Zhang, K. Y. J. Keynote review: Phosphodiesterase-4 as a therapeutic target. *Drug Discovery Today* **2005**, *10*, 1503−1519.

(10) Wang, D. G; Deng, C. J.; Bugaj-Gaweda, B.; Kwan, M.; Gunwaldsen, C.; Leonard, C.; Xin, X. N.; Hu, Y. H.; Unterbeck, A.; De Vivo, M. Cloning and characterization of novel PDE4D isoforms PDE4D6 and PDE4D7. *Cell. Signalling* **2003**, *15*, 883−891.

(11) Castro, A.; Jerez, M. J.; Gil, C.; Martinez, A. Cyclic nucleotide phosphodiesterases and their role in immunomodulatory responses: Advances in the development of specific phosphodiesterases inhibitors. *Med. Res. Rev.* **2005**, *25*, 229−244.

(12) Banner, K. H.; Trevethick, M. A. PDE4 inhibition: A novel approach for the treatment of inflammatory bowel disease. *Trends Pharmacol. Sci.* **2004**, *25*, 430−436.

(13) Draheim, R.; Egerland, U.; Rundfeldt, C. Anti-inflammatory potential of the selective phosphodiesterase 4 inhibitor N-(3,5-dichloro-pyrid-4-yl)-[1-(4-fluorobenzyl)-5-hydroxy-indole-3-yl]-glyoxylic acid amide (AWD 12−281), in human cell preparations. *J. Pharmacol. Exp. Ther.* **2004**, *308*, 555−563.

(14) Jeffery, P. Phosphodiesterase 4-selective inhibition: Novel therapy for the inflammation of COPD. *Pulm. Pharmacol. Ther.* **2005**, *18*, 9−17.

(15) O'Donnell, J. M.; Zhang, H. Antidepressant effects of inhibitors of cAMP phosphodiesterase (PDE4). *Trends Pharmacol. Sci.* **2004**, *25*, 158−163.

(16) Spina, D. The potential of PDE4 inhibitors in respiratory disease. *Curr. Drug Targets: Inflammation Allergy* **2004**, *3*, 231−236.

(17) O'Byrne, P. M.; Gauvreau, G. Phosphodiesterase-4 inhibition in COPD. *Lancet* **2009**, *374*, 665−667.

(18) Pages, L.; Gavalda, A.; Lehner, M. D. PDE4 inhibitors: A review of current developments (2005−2009). *Expert Opin. Ther. Pat.* **2009**, *19*, 1501−1519.

(19) Page, C. P.; Spina, D. Selective PDE inhibitors as novel treatments for respiratory diseases. *Curr. Opin. Pharmacol.* **2012**, *12*, 1−12.

(20) Kodimuthali, A.; Jabaris, S. S. L.; Pal, M. Recent advances on phosphodiesterase 4 inhibitors for the treatment of asthma and chronic obstructive pulmonary disease. *J. Med. Chem.* **2008**, *51*, 5471−5489.

(21) Amschler, H. Fluoroalkoxy-substituted benzamides and their use as cyclic nucleotide phosphodiesterase inhibitors. US Patent 5,712,298, 1998.

(22) Fabbri, L. M.; Calverley, P. M. A.; Izquierdo-Alonso, J. L.; Bundschuh, D. S.; Brose, M.; Martinez, F. J.; Rabe, K. F. Roflumilast in moderate-to-severe chronic obstructive pulmonary disease treated with longacting bronchodilators: Two randomised clinical trials. *Lancet* **2009**, *374*, 695−703.

(23) Hatzelmann, A.; Morcillo, E. J.; Lungarella, G.; Adnot, S.; Sanjar, S.; Beume, R.; Schudt, C.; Tenor, H. The preclinical pharmacology of roflumilast - A selective, oral phosphodiesterase 4 inhibitor in development for chronic obstructive pulmonary disease. *Pulm. Pharmacol. Ther.* **2010**, *23*, 235−256.

(24) Calverley, P. M. A.; Rabe, K. F.; Goehring, U. M.; Kristiansen, S.; Fabbri, L. M.; Martinez, F. J. Roflumilast in symptomatic chronic obstructive pulmonary disease: Two randomised clinical trials. *Lancet* **2009**, *374*, 685−694.

(25) Duplantier, A. J.; Bachert, E.; Cheng, J.; Cohan, V.; Jenkinson, T.; Kraus, K.; McKechney, M.; Pillar, J.; Watson, J. SAR of a series of 5,6-dihydro-(9H)-pyrazolo[3,4-c]-1,2,4-triazolo[4,3-α]pyridines as potent inhibitors of human eosinophil phosphodiesterase. *J. Med. Chem.* **2007**, *50*, 344−349.

(26) Robichaud, A.; Stamatiou, P. B.; Jin, C.; Lachance, N.; MacDonald, D.; Laliberté, F.; Liu, S.; Huang, Z.; Conti, M.; Chan, C. C. Deletion of phosphodiesterase 4D in mice shortens alpha2-adrenoceptor-mediated anesthesia, a behavioural correlate of emesis. *J. Clin. Invest.* **2002**, *110*, 1045−1052.

(27) Dal Piaz, V.; Giovannoni, M. P. Phosphodiesterase 4 inhibitors, structurally unrelated to rolipram, as promising agents for the treatment of asthma and other pathologies. *Eur. J. Med. Chem.* **2000**, *35*, 463−480.

(28) Houslay, M. D.; Adams, D. R. Putting the lid on phosphodiesterase 4. *Nat. Biotechnol.* **2010**, *28*, 38−40.

(29) Giembycz, M. A. 4D or not 4D − the emetogenic basis of PDE4 inhibitors uncovered? *Trends Pharmacol. Sci.* **2002**, *23*, 548.

(30) Giembycz, M. A.; Field, S. K. Roflumilast: The first in class phosphodiesterase 4 inhibitor approved for the treatment of COPD. *Drug Des., Dev. Ther.* **2010**, *4*, 147−158.

(31) Fraga, C. A. M.; Barreiro, E. J. Medicinal chemistry of N-acylhydrazones: New lead-compounds of analgesic, antiinflammatory and antithrombotic drugs. *Curr. Med. Chem.* **2006**, *13*, 167−198.

(32) Duarte, C. D.; Barreiro, E. J.; Fraga, C. A. M. Privileged structures: A useful concept for the rational design of new lead drugs candidates. *Mini-Rev. Med. Chem.* **2007**, *7*, 1108−1119.

(33) Fraga, C. A. M.; Barreiro, E. J. Cardiotônicos: Histórico e perspectivas de uma antiga e importante classe de agentes terapêuticos. *Quim. Nova* **1996**, *19*, 182−189.

(34) Barreiro, E. J. Estratégia de simplificação molecular no planejamento racional de fármacos: A descoberta de novo agente cardioativo. *Quim. Nova* **2002**, *25*, 1172−1180.

(35) Sudo, R. T.; Zapata-Sudo, G.; Barreiro, E. J. LASSBio 294, a novel cardionotropic agent, increases the calcium content in the sarcoplasmatic reticulum of saponin-skinned cardiac fibres. *Br. J. Pharmacol.* **2001**, *134*, 603−613.

(36) Silva, C. L. M.; Noel, F.; Barreiro, E. J. Vasodilatory properties of LASSBio 294 and its dependence on cGMP increase. *Br. J. Pharmacol.* **2002**, *135*, 293−298.

(37) Dal Piaz, V.; Giovannoni, M.; Castellana, C.; Palacios, J.; Beleta, J.; Domenech, T.; Segarra, V. Heterocyclic-fused 3(2H)-pyridazinones as potent and selective PDE IV inhibitors: Further structure−activity relationships and molecular modelling studies. *J. Med. Chem.* **1997**, *40*, 1417−1421.

(38) Lima, L. M.; Barreiro, E. J. Bioisosterism, an useful strategy for molecular modification and drug design. *Curr. Med. Chem.* **2005**, *12*, 23−49.

(39) Kümmerle, A. E.; Raimundo, J. M.; Leal, C. M.; da Silva, G. S.; Balliano, T. L.; Pereira, M. A.; de Simone, C. A.; Sudo, R. T.; Zapata-Sudo, G.; Fraga, C. A.; Barreiro, E. J. Studies towards the identification of putative bioactive conformation of potent vasodilator arylidene N-acylhydrazone derivatives. *Eur. J. Med. Chem.* **2009**, *44*, 4004−4009.

(40) Silva, A. G.; Zapata-Sudo, G.; Kummerle, A. E.; Fraga, C. A. M.; Barreiro, E. J.; Sudo, R. T. Synthesis and vasodilatory activity of new N-acylhydrazone derivatives, designed as LASSBio-294 analogues. *Bioorg. Med. Chem.* **2005**, *13*, 3431−3437.

(41) Yamada, S.; Morizono, D.; Yamamoto, K. Mild oxidation of aldehydes to the corresponding carboxylic acids and esters: Alkaline iodine oxidation revisited. *Tetrahedron Lett.* **1992**, *33*, 4329−4332.

(42) Lima, P. C.; Lima, L. M.; da Silva, K. C. M.; Léda, P. H. O.; de Miranda, A. L. P.; Fraga, C. A. M.; Barreiro, E. J. Synthesis and analgesic activity of novel N-acylhydrazones and isosters, derived from natural safrole. *Eur. J. Med. Chem.* **2000**, *35*, 187−203.

(43) Lai, G.; Anderson, W. K. A simplified procedure for the efficient conversion of aromatic aldehydes into esters. *Synth. Commun.* **1997**, *27*, 1281−1283.

(44) Kaminski, J. J.; Bristol, J. A.; Puchalski, C.; Lovey, R. G.; Elliott, A. J.; Guzik, H.; Solomon, D. M.; Conn, D. J.; Domalski, M. S.

Antiulcer agents. 1. Gastric antisecretory and cytoprotective properties of substituted imidazo[1,2-*a*]pyridines. *J. Med. Chem.* **1985**, *28*, 876−892.

(45) Ribeiro, I. G.; da Silva, K. C. M.; Parrini, S. C.; de Miranda, A. L. P.; Fraga, C. A. M.; Barreiro, E. J. Synthesis and antinociceptive properties of new structurally planned imidazo[1, 2-*a*]pyridine 3-acylarylhydrazone derivatives. *Eur. J. Med. Chem.* **1998**, *33*, 225−235.

(46) Patel, J. M.; Dave, M. P.; Langalia, N. A.; Thaker, K. A. Studies on antitubercular agents preparation of 1-(4-methoxybenzoyl)-2-benzalhydrazine and 2-aryl-3-(4-methoxybenzamido)-5-carboxymethyl-4-thiazolidinone. *J. Indian Chem. Soc.* **1985**, *62*, 254−255.

(47) Kumar, P.; Narasimhan, B.; Sharma, D.; Judge, V.; Narang, R. Hansch analysis of substituted benzoic acid benzylidene/furan-2-yl-methylene hydrazides as antimicrobial agents. *Eur. J. Med. Chem.* **2009**, *44*, 1853−1863.

(48) Kumar, D.; Narang, R.; Judge, V.; Kumar, D.; Narasimhan, B. Antimicrobial evaluation of 4-methylsulfanyl benzylidene/3-hydroxy benzylidene hydrazides and QSAR studies. *Med. Chem. Res.* **2012**, *21*, 382−394.

(49) Karabatsos, G. J.; Taller, R. A. Structural studies by nuclear magnetic resonance. V. Phenylhydrazones. *J. Am. Chem. Soc.* **1963**, *85*, 3624−3629.

(50) Palla, G.; Predieri, G.; Domiano, P.; Vignali, C.; Turner, W. Conformational behaviour and *E/Z* isomerization of *N*-acyl and *N*-aroylhydrazones. *Tetrahedron* **1986**, *42*, 3649−3654.

(51) Palla, G.; Pelizzi, C.; Predieri, G.; Vignali, C. Conformational study on *N*-acylhydrazones of aromatic-aldehydes by NMR-spectroscopy. *Gazz. Chim. Ital.* **1982**, *112*, 339−341.

(52) Barco, A.; Benetti, S.; Pollini, G. P. A facile alkylation of ethyl 2-oxocyclopentanecarboxylate. *Synthesis* **1973**, 316.

(53) Benstead, D. J.; Hulme, A. N.; McNab, H.; Wight, P. An efficient synthesis of substituted hydrazides. *Synlett* **2005**, 1571−1574.

(54) Spivey, A. C.; McKendrick, J.; Srikaran, R.; Helm, B. A. Solid-phase synthesis of an A−B loop mimetic of the C epsilon 3 domain of human IgE: Macrocyclization by Sonogashira coupling. *J. Org. Chem.* **2003**, *68*, 1843−1851.

(55) Hellal, M.; Bourguignon, J.; Bihel, F. J. 6-*endo-dig* Cyclization of heteroarylesters to alkynes promoted by Lewis acid catalyst in the presence of Brönsted acid. *Tetrahedron Lett.* **2008**, *49*, 62−65.

(56) Lugnier, C.; Schoeffter, P.; Le Bec, A.; Strouthou, E.; Stoclet, J. C. Selective inhibition of cyclic nucleotide phosphodiesterases of human, bovine and rat aorta. *Biochem. Pharmacol.* **1986**, *35*, 1743−1751.

(57) Tcheudji, J. F. K.; Lebeau, L.; Virmaux, N.; Maftei, C. G.; Cote, R. H.; Lugnier, C.; Schultz, P. Molecular organization of bovine rod cGMP-phosphodiesterase 6. *J. Mol. Biol.* **2001**, *310*, 781−791.

(58) Keravis, T. M.; Wells, J. N.; Hardman, J. G. Cyclic nucleotide phosphodiesterase activities from pig coronary arteries. Lack of interconvertibility of major forms. *Biochim. Biophys. Acta* **1980**, *613*, 116−129.

(59) Barreiro, E. J.; Kümmerle, A. E.; Fraga, C. A. M. The methylation effect in medicinal chemistry. *Chem. Rev.* **2011**, *111*, 5215−5246.

(60) Lagente, V.; Martin-Chouly, C.; Boichot, E.; Martins, M. A.; Silva, P. M. Selective PDE4 inhibitors as potent anti-inflammatory drugs for the treatment of airway diseases. *Mem. Inst. Oswaldo Cruz* **2005**, *100* (Suppl 1), 131−136.

(61) Robichaud, A.; Savoie, C.; Stamatiou, P. B.; Tattersall, F. D.; Chan, C. C. PDE4 inhibitors induce emesis in ferrets via a noradrenergic pathway. *Neuropharmacology* **2001**, *40*, 262−269.

(62) Robichaud, A.; Savoie, C.; Stamatiou, P. B.; Lachance, N.; Jolicoeur, P.; Rasori, R.; Chan, C. C. Assessing the emetic potential of PDE4 inhibitors in rats. *Br. J. Pharmacol.* **2002**, *135*, 113−118.

(63) Williams, R. O.; Feldmann, M.; Maini, R. N. Anti-tumor necrosis factor ameliorates joint disease in murine collagen-induced arthritis. *Proc. Natl. Acad. Sci. U.S.A.* **1992**, *89*, 9784−9788.

(64) Barnes, P. J. Cytokines as mediators of chronic asthma. *Am. J. Respir. Crit. Care Med.* **1994**, *150*, 542−549.

(65) Renzetti, L. M.; Paciorek, P. M.; Tannu, S. A.; Rinaldi, N. C.; Tocker, J. E.; Wasserman, M. A.; Gater, P. R. Pharmacological evidence for tumor necrosis factor as a mediator of allergic inflammation in the airways. *J. Pharmacol. Exp. Ther.* **1996**, *278*, 847−853.

(66) Jin, S. L.; Conti, M. Induction of the cyclic nucleotide phosphodiesterase PDE4B is essential for LPS-activated TNF-alpha responses. *Proc. Natl. Acad. Sci. U.S.A.* **2002**, *99*, 7628−7633.

(67) Hartman, D. A.; Ochalski, S. J.; Carlson, R. P. The effects of antiinflammatory and antiallergic drugs on cytokine release after stimulation of human whole blood by lipopolysaccharide and zymosan A. *Inflamm. Res.* **1995**, *44*, 269−274.

(68) Heaslip, R. J.; Evans, D. Y. Emetic, central nervous system and pulmonary activities of rolipram in the dog. *Eur. J. Pharmacol.* **1995**, *286*, 281−290.

(69) Lagente, V.; Martin-Chouly, C.; Boichot, E.; Martins, M. A.; Silva, P. M. R. Selective PDE4 inhibitors as potent anti-inflammatory drugs for the treatment of airway diseases. *Mem. Inst. Oswaldo Cruz* **2005**, *100*, 131−136.

(70) Harmsen, A. Role of alveolar macrophages in lipopolysaccharide-induced neutrophil accumulation. *Infect. Immun.* **1988**, *56*, 1858−1863.

(71) Horn, R. G.; Collins, R. D. Fragmentation of granulocytes in pulmonary capillaries during development of the generalized Shwartzman reaction. *Lab. Invest.* **1968**, *19*, 451−459.

(72) O'Malley, J.; Matesic, L. E.; Zink, M. C.; Strandberg, J. D.; Mooney, M. L.; De Maio, A.; Reeves, R. H. Comparison of acute endotoxin-induced lesions in A/J and C57BL/6J mice. *J. Hered.* **1998**, *89*, 525−530.

(73) Gonçalves de Moraes, V. L.; Vargaftig, B. B.; Lefort, J.; Meager, A.; Chignard, M. Effect of cyclo-oxygenase inhibitors and modulators of cyclic AMP formation on lipopolysaccharide-induced neutrophil infiltration in mouse lung. *Br. J. Pharmacol.* **1996**, *117*, 1792−1796.

(74) McKay, D. G.; Margaretten, W.; Csavossy, I. An electron microscope study of the effects of bacterial endotoxin on the blood-vascular system. *Lab. Invest.* **1966**, *15*, 1815−1829.

(75) McCaffree, D. R.; Gray, B. A.; Pennock, B. E. Role of pulmonary edema in the acute pulmonary response to sepsis. *J. Appl. Physiol.* **1981**, *50*, 1198−1205.

(76) Olson, N.; Brown, T., Jr.; Anderson, D. Effect of polyethylene glycol-superoxide dismutase and catalase on endotoxemia in pigs. *J. Appl. Physiol.* **1985**, *58*, 274−284.

(77) Meyrick, B.; Brigham, K. L. Acute effects of *E. coli* endotoxin on the pulmonary microcirculation of anesthetized sheep. *Lab. Invest.* **1983**, *48*, 458−470.

(78) Coalson, J. J.; Hinshaw, L. B.; Guenter, C. A. The pulmonary ultrastructure in septic shock. *Exp. Mol. Pathol.* **1970**, *12*, 84−103.

(79) Burch, R. M.; Noronha-Blob, L.; Bator, J. M.; Lowe, V. C.; Sullivan, J. P. Mice treated with a leumedin or antibody to Mac-1 to inhibit leukocyte sequestration survive endotoxin challenge. *J. Immunol.* **1993**, *150*, 3397−3403.

(80) Golec, M. Cathelicidin LL-37: LPS-neutralizing, pleiotropic peptide. *Ann. Agric. Environ. Med.* **2007**, *14*, 1−4.

(81) Tralau-Stewart, C. J.; Williamson, R. A.; Nials, A. T.; Gascoigne, M.; Dawson, J.; Hart, G. J.; Angell, A. D. R.; Solanke, Y. E.; Lucas, F. S.; Wiseman, J.; Ward, P.; Ranshaw, L. E.; Knowles, R. G. GSK256066, an exceptionally high-affinity and selective inhibitor of phosphodiesterase 4 suitable for administration by inhalation: in vitro, kinetic, and in vivo characterization. *J. Pharmacol. Exp. Ther.* **2011**, *337*, 145−154.

(82) Spond, J.; Chapman, R.; Fine, J.; Jones, H.; Kreutner, W.; Kung, T. T.; Minnicozzi, M. Comparison of PDE 4 inhibitors, rolipram and SB 207499 (Ariflo^TM), in a rat model of pulmonary neutrophilia. *Pulm. Pharmacol. Ther.* **2001**, *14*, 157−164.

(83) Lefort, J.; Singer, M.; Leduc, D.; Renesto, P.; Nahori, M. A.; Huerre, M.; Créminon, C.; Chignard, M.; Vargaftig, B. B. Systemic administration of endotoxin induces bronchopulmonary hyper-reactivity dissociated from TNF-alpha formation and neutrophil sequestration into the murine lungs. *J. Immunol.* **1998**, *161*, 474−480.

(84) Evers, A.; Klebe, G. Ligand-supported homology modeling of G-protein-coupled receptor sites: models sufficient for successful virtual screening. *Angew. Chem., Int. Ed.* **2004**, *43*, 248−251.

(85) Card, G. L.; England, B. P.; Suzuki, Y.; Fong, D.; Powell, B.; Lee, B.; Luu, C.; Tabrizizad, M.; Gillette, S.; Ibrahim, P. N.; Artis, D. R.; Bollag, G.; Milburn, M. V.; Kim, S. H.; Schlessinger, J.; Zhang, K. Y. Structural basis for the activity of drugs that inhibit phosphodiesterases. *Structure* **2004**, *12*, 2233−2247.

(86) Case, D. A.; Cheatham, T. E., III; Darden, T.; Gohlke, H.; Luo, R.; Merz, K. M., Jr.; Onufriev, A.; Simmerling, C.; Wang, B.; Woods, R. The Amber biomolecular simulation programs. *J. Comput. Chem.* **2005**, *26*, 1668−1688.

(87) Kagechika, H.; Himi, T.; Kawachi, E.; Shudo, K. Retinobenzoic acids. 4. Conformation of aromatic amides with retinoidal activity. Importance of *trans*-amide structure for the activity. *J. Med. Chem.* **1989**, *32*, 2292−2296.

(88) Kümmerle, A. E.; Vieira, M. M.; Schmitt, M.; Miranda, A. L.; Fraga, C. A.; Bourguignon, J.; Barreiro, E. J. Design, synthesis and analgesic properties of novel conformationally-restricted *N*-acylhydrazones (NAH). *Bioorg. Med. Chem. Lett.* **2009**, *19*, 4963−4966.

(89) Tobe, M.; Isobe, Y.; Tomizawa, H.; Nagasaki, T.; Takahashi, H.; Fukazawa, T.; Hayashi, H. Discovery of quinazolines as a novel structural class of potent inhibitors of NF-[kappa]B activation. *Bioorg. Med. Chem.* **2003**, *11*, 383−391.

(90) Gineinah, M. M.; Ismaiel, A. E. M.; El-Kerdawy, M. M.; Glennon, R. A. Mesoionic 1,2,4-triazolo[4,3-c]quinazolines. *J. Heterocycl. Chem.* **1990**, *27*, 723−726.

(91) Collot, V.; Dallemagne, P.; Bovy, P. R.; Rault, S. Suzuki-type cross-coupling reaction of 3-iodoindazoles with aryl boronic acids: A general and flexible route to 3-arylindazoles. *Tetrahedron* **1999**, *55*, 6917−6922.

(92) Böyum, A. Isolation of mononuclear cells and granulocytes from human blood. Isolation of monuclear cells by one centrifugation, and of granulocytes by combining centrifugation and sedimentation at 1 g. *Scand. J. Clin. Lab. Invest. Suppl.* **1968**, *97*, 77−89.

(93) Reimund, J. M.; Wittersheim, C.; Dumont, S.; Muller, C. D.; Kenney, J. S.; Baumann, R.; Poindron, P.; Duclos, B. Increased production of tumour necrosis factor-alpha interleukin-1 beta, and interleukin-6 by morphologically normal intestinal biopsies from patients with Crohn's disease. *Gut* **1996**, *39*, 684−689.

(94) Sybyl, Version 7.3. Tripos Associates: St. Louis, MO, 2007.

(95) Halgren, T. A. Merck molecular force field. II. MMFF94 van der Waals and electrostatic parameters for intermolecular interactions. *J. Comput. Chem.* **1996**, *17*, 520−552.

(96) Dewar, M. J. S.; Zoebisch, E. G.; Healy, E. F.; Stewart, J. J. P. Development and use of quantum mechanical molecular models. 76. AM1: a new general purpose quantum mechanical molecular model. *J. Am. Chem. Soc.* **1985**, *107*, 3902−3909.